Integrated use and interpretation of data from different geophysical methods for site investigation for underground construction

Mathias Ronczka, Roger Wisén,
Torleif Dahlin & Kristofer Hellman

LUND
UNIVERSITY

Faculty of Engineering| Engineering Geology

ISRN LUTVDG/(TVTG-3101)/1-30/2016

Lund 2016

Abstract

Unforeseen ground conditions are risk factors that often lead to significant delays and additional costs associated with the construction of underground facilities. The purpose of this project is the development, testing and demonstration of methods for integrated use and interpretation of data from different geophysical measurements and in situ methods such as drilling, etc. to create improved forecasting models for the investigation of soil and rock properties. This is be done with selected underground construction projects as application examples. The engineering geological forecast model should provide information on the rock mass, rock quality and uncertainty in these parameters.

The work includes the development, adaptation and evaluation of software to create models of the ground by data from different survey methods that are weighted together. By combining data from various geophysical and non-geophysical methods, it is possible to reduce the uncertainties and create more reliable models. Calibration and evaluation of methodologies and algorithms are made against synthetic model data. The work also includes field survey to collect data from relevant geological environments adjacent to existing and planned underground caverns or construction. The collected data are used for test and calibration of the developed methods.

Field trials have to date been carried out in connection with the ESS in Lund, Kv Färgaren in Kristianstad, the Varberg tunnel, Äspö HRL Önneslöv-Dalby, Stockholm Bypass at Lambarfjärden and Östlig förbindelse.

Preface

The work of this thesis has been carried out at the Division of Engineering Geology, Lund University in Sweden and in part at the TRUST 4.2 project "Integrated Use and Interpretation of Data from Geophysical and Non-Geophysical Methods for Site Investigation for Underground Construction". The project is part of the Geoinfra-TRUST framework (http://www.trust-geoinfra.se/).

Funding for the project has been provided by BeFo - Swedish Rock Engineering Research Foundation, (ref. 314) and SBUF - The Development Fund of the Swedish Construction Industry, (ref. 12718). Furthermore Byggrådet provided funding for Roger Wisén's participation. In addition Nova FOU provided essential economic support the field campaign. Leibniz Institute for Applied Geophysics (LIAG) and Lund University (LU) provided in-kind support. Formas provided funding for Kristofer Hellman via the GESP project.

We are grateful for the fruitful collaboration with the other participants within the TRUST framework. Furthermore we want to than SKB for valuable support and nice collaboration in connection with the Äspö field test.

The Authors

February 2016

Contents

1 Introduction

1.1 Overview

This report presents preliminary results achieved within a project which is a part of the TRUST (TRansparent Underground STructure) framework. The background of the TRUST project springs from an urgent need to build more cost efficient underground structures. While keeping costs at a minimum, the demands for sustainable, safe and easily maintainable underground structures are not to be neglected. Lifecycle costs for the structures must be taken into account. A significant driver for this is a recent development of stricter national and European regulations on energy and environment. The overall vision of the TRUST project is to:

- Promote research on development of sustainable urban underground infrastructure design
- Develop improved methods and tools for better planning, design and construction of urban underground structures

The TRUST framework consists of a set of subprojects focusing on holistic site investigation methods (TRUST 2.1, 2.2, 2.3 and 2.4), smart underground construction (TRUST 3.1, 3.2 and 3.3) and information models, data structure and visualization (TRUST 4.1 and 4.2). The structure of the TRUST framework is shown in Figure 1.

Subproject TRUST 4.2 deals with integrated use and interpretation of data from geophysical and non-geophysical methods for site investigation. A well-functioning site investigation process is needed, in order to reduce costs, the risk for delays and an unnecessary impact on the environment. To achieve this, it is important to work on the development and adaption of an improved methodology for combining geological and geophysical properties to increase the reliability of rock mass and rock quality evaluation. The approach of joint interpretation and inversion of geophysical and non-geophysical data sets lead to more reliable subsurface models and thus a better prediction of rock mass and rock quality. Furthermore, the aim is to develop the usability of geophysical methods by presenting a model that not only shows the magnitude of the physical properties but also the uncertainty in these.

The development of geophysical methodology to support civil engineering projects has been developing since the late 1970's. The bulk of the scientific methods and equations have been in place before the civil engineering applicability was even considered. The development and fast evolution of the microprocessor spilled over to the geophysical community and helped to evolve most parts of the data collection and evaluation. The methodologies moved from 1D sounding to 2D, 3D and 4D (monitoring over time). In order for geophysics to reach its full potential in civil engineering applications, there is a need for geotechnical parameters to be directly or indirectly attained by the methods. Geophysical methods have already proved useful in many civil engineering projects (e.g. Dahlin et al. (1999), Cavinato et al. (2006), Danielsen et al. (2007) and Wang (2010)).

Soil and bedrock mechanical properties are the primary focus of a geotechnical site investigation. By tradition, these properties are attained by probing and sounding methods.

These methods provide 1D information that is very accurate and precise; there is however the problem of the 1D-approach is that it is not possible to simply extend the information to 3D, which is most often necessary to describe an environment properly. At this stage, geophysical methods could be used to shed some light and provide an overview of the situation. However, this does not in any way exclude the need for the traditional probing and sounding. The increasing overall complexity of many civil engineering projects could possibly benefit from geophysics to establish an early understanding and identify zones of interest. In order to facilitate this understanding, the geophysical methods need to be cost effective and relatively easy to understand for someone who is not a professional geophysicist.

This work addresses integrated interpretation between different types of geophysical data. The use of more than one method can be motivated by using an analogy to the human sensory apparatus. In order to deduce the true nature of our surrounding, we need to use several of our sensory impressions (or data input) to produce a credible opinion about our reality. With experience, we can also deduce that it's just another apple that we are first looking at, touching, smelling and finally tasting. With our geophysical instruments and geotechnical methods, we can locate and classify a possible fault zone without excavating the entire thing.

The concept of joint inversion of geophysical data was first introduced by Vozoff & Jupp (1975), their main motivation being the ability to avoid ambiguities following the use of a single method on its own. There are several ways to obtain multiple data for a description of the substrata.

I) Collecting several datasets with several methods that sense the same geophysical properties (e.g. Sasaki 1989),

II) Collecting several datasets with several methods that sense different geophysical properties (e.g. Lines et al. 1988).

Using the first approach can be motivated by the fact that some methods have different resolution with depth and that several methods for a single parameter can facilitate a better overall resolution of a model. Using the second approach may be motivated by one methods ability to detect e.g one specific material layer boundary, while another method can detect fissures that may appear in the interface. Whatever reason, if the information obtained by several geophysical can be more useful while used in cooperation; this could be a good reason for the recovery of this information.

After the collection of site specific geophysical data has been carried out, there are three main approaches for processing the data to create a unified site description.

1) Manual joint interpretation, the interpreter uses the data and experience to create a unified model.

2) Inversion methods that employs hydrological or petrophysical links to relate the geophysical properties to each other (e.g. Tryggvason and Flóvenz 2002), the links are often unknown and affected by a multitude of rock properties, including state variables regarding these properties (e.g. Nur et al. 1998).

3) The structural approach, which is based on the assumption that near surface geophysical properties are co-dependent from a structural viewpoint (Haber and Oldenburg 1997; Gallardo and Meju 2004; Linde et al. 2008).

By assuming that the changes in the geophysical parameters occur in the same direction, changes are calculated by the use of a function. This function, referred to as the cross-gradient function, enables quantification of structural similarities between two separate models. Yet another approach, presented by Auken and Christiansen (2004) was extended by Juhojuntti and Kamm (2015), using sharp boundary models from different methods to constrain another method.

A major concern for someone who is not familiar with the joint inversion methods may be that the method can produce either one final model or one model for each method. Generally, when employing geophysical methods sensitive to the same physical parameter, the result is a single model. Conversely, when employing geophysical methods that are sensitive to different physical properties, the result is one model per geophysical method. In order to facilitate automated interpretation of the latter, the use of a statistical tool such as cluster analysis could prove useful (e.g. Tronicke et al. 2994; Paasche et al. 2006; Dietrich and Tronicke 2009).

1.2 Aims and delimitations

The aim is to develop and adapt methods for combined analysis and interpretation of geophysical, geological and geotechnical data in an efficient and objective manner. The aim is to develop the practical applicability of geophysical methods by making models that not only shows the magnitude of the (geo)physical properties, but also the uncertainty of these. Furthermore, the aim is to develop and evaluate techniques for objective co-interpretation of geophysical and non-geophysical data in order to create better mountain forecasts (geological expectation models) with the analysis of the uncertainty in the models (risk analysis) included.

The goal is to adapt, develop and evaluate methods for the so-called coupled (or joint) inversion (inverse numerical modeling). The focus regarding geophysical techniques will be limited to resistivity, IP effect (induced polarization = chargeability) and seismic p-wave velocity, because it deemed the most practical applicable. Furthermore, the goal is to adapt the interpretation methods to integrate different types of data from drilling and other in-situ investigations.

The expected outcome of the project is a new method for creating a basis for improved engineering geological models (rock quality forecasts) based on co-interpreted geophysical and other data. The models will provide information on the distribution of the characteristics of the rock mass, rock quality and uncertainty of these.

1.3 Implementation and progress

The project is built up of different activities that include adaption, development, testing and evaluation of methods and software as well as field tests.

The used interpretation software used is GIMLi (Geophysical Inverse Modelling Library) which is an open source software library. The work builds on existing algorithms that are developed in collaboration with leading researchers in our international research network. Extensive work has been done to adapt, develop, organize, improve and document the program code so that we now have an efficient tool for the continued work.

Work on the development of methodology for the analysis and presentation of the reliability of the interpretation models have started and used for internal testing. Methods for visualizing models that fade out to be more transparent with increasing uncertainty has been tested but it needs to be further tested and refined.

Extensive work with testing of the algorithms against synthetic data examples based on different geological scenarios have been carried out. Field tests have been made at for example Förbifart Stockholm, Äspö hard rock laboratory and the Varberg tunnel in close cooperation with other TRUST projects that carry out geophysical test with other methods. The chosen test sites provide the opportunity to get access to a large variety of reference data that include core drilling and logging, geologic information and laboratory analyses. Field trials have in addition been carried out in connection with the ESS in Lund, Kv Färgaren in Kristianstad, the Önneslöv-Dalby, and Östlig förbindelse. We have also worked with geophysical pre-investigation data from E16 in Norway.

2 Method description

The key point of the project is to combine different geophysical methods, to enhance the reliability of estimated subsurface models. The most important geophysical methods in this study are resistivity, IP (Induced Polarization), seismic refraction and magnetic field data. In the following the two methods that have been in focus in the first two years of the study, ERT and seismic refraction, are explained. A section on inverse modelling will point out the methodology of estimating a parameter distribution that describes the subsurface on the basis of measured data, and especially a description is given of how the data of two different geophysical methods can be combined by joint inverse modelling. Finally, the fundamentals of an objective tool for interpretation with means of cluster analysis will be described.

2.1 Electrical Resistivity Tomography (ERT)

Electrical resistivity tomography dates back to the early 1900s. The method came into wide use in the 1970s. The development of the method largely follows the evolution of the modern computers as this is needed for the processing and analysis of the data. The applied method within this report is direct current resistivity.

The fundamental physical law used for resistivity measurements is Ohms law:

$$U = R \cdot I \qquad (1)$$

Where U is the voltage in volts, R is the resistance in Ohms and I is the current in A. It describes that the current, which flows through a conductor is directly proportional to the potential difference, i.e. voltage between two points. This is directly applicable to ideal electrical components. Another well-known form, seen from a local point of view is j=σE, with the current density j [A/m^2], the electrical field E [V/m] and the electrical conductivity σ. An ERT measurement is carried out by using several four-point electrode combinations with a changing electrode spacing. A schematic sketch of a four-point electrode array is shown in Figure 1.

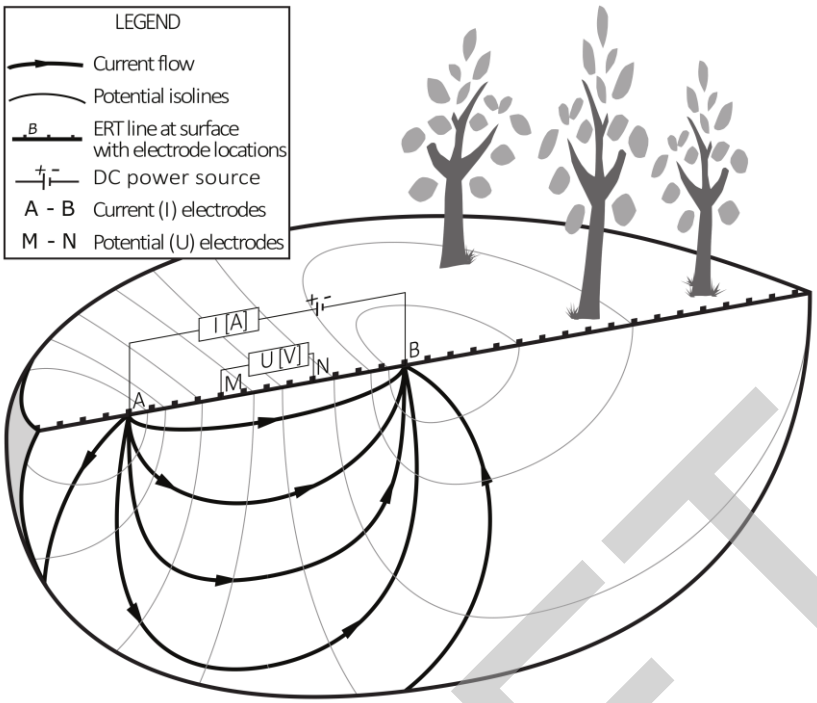

Figure 1. Schematic overview of DC resistivity measurement principle on a homogenous subsurface. Original image provided by Nijland et al. (2010).

The four-electrode scheme can be used to estimate the electrical resistivity (ρ, in Ωm). A representative resistivity is calculated by assuming a homogeneous and isotropic subsurface and taking in to account the distances between the electrodes. This resistivity is referred to as the apparent resistivity,

$$\rho_a = K\frac{U}{I} \qquad (2)$$

where

$$K = 2\pi(r_{AM}^{-1} - r_{BM}^{-1} - r_{AN}^{-1} - r_{BN}^{-1})^{-1}$$

is called geometric factor and *r* denotes the distances between the electrodes, A and B are electrical current electrodes and M N are electrical potential electrodes. Hereby, the investigation depth of a single measurement is controlled by the distance between electrodes. Most commonly 2D ERT measurements are carried out along profiles, to image a heterogeneous resistivity distribution. Several electrodes are placed along a profile line, which are wired and controlled by an apparatus that automatically transmits the current and measures the voltage following a pre-defined scheme, for example a Wenner-α or Dipole-Dipole array. The geometry of each measurement is considered by multiplying each resistivity with its geometric factor K. The obtained data are called apparent resistivities ρ_a, because they are an integral value and not assigned to a specific depth. In order to estimate a resistivity distribution that explains the measured data within a realistic error model an inversion is needed.

Modern data acquisition systems employ micro computer controlled multi-electrode arrays as shown in figure 2 (e.g. Dahlin 2001). Once the electrode spread is laid out the instrument measures the contact resistances to ensure that sufficiently good galvanic contact has been established between the electrode and the ground, and reports where improvement is needed. When sufficient contact is established the instrument scans though a pre-defined measurement protocol which typically consists of many hundreds or thousands of data points (four electrode combinations). The measured data are interpreted with the help of inversion (see section below).

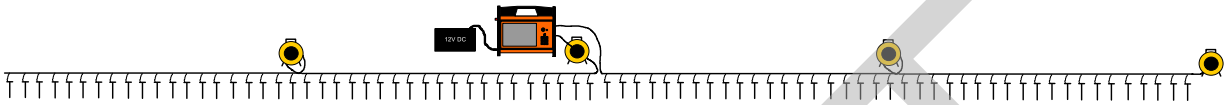

Figure 2. Example of the typical electrode spread for 2D ERT consisting of four electrode cables linked together along a line.

2.2 Induced Polarisation

The electrical resistivity of most geologic material shows a decaying voltage after a current pulse has been turned off, which is caused by polarisation effects. Originally developed for ore exploration it has proven to be useful, by giving additional and sometimes more detailed information about geologic conditions than resistivity alone. The induced polarisation (IP) method measures the chargeability which is a material property that quantifies the capacity of the material to store electrical energy. In time-domain IP the chargeability is defined as the ratio between the measured voltage following a sudden change in current ($V_{IP,0}$, Figure 3), normalized with the measured potential before the current change (V_{DC}) (Seigel, 1959):

$$m_0 = \frac{V_{IP,0}}{V_{DC}}.$$

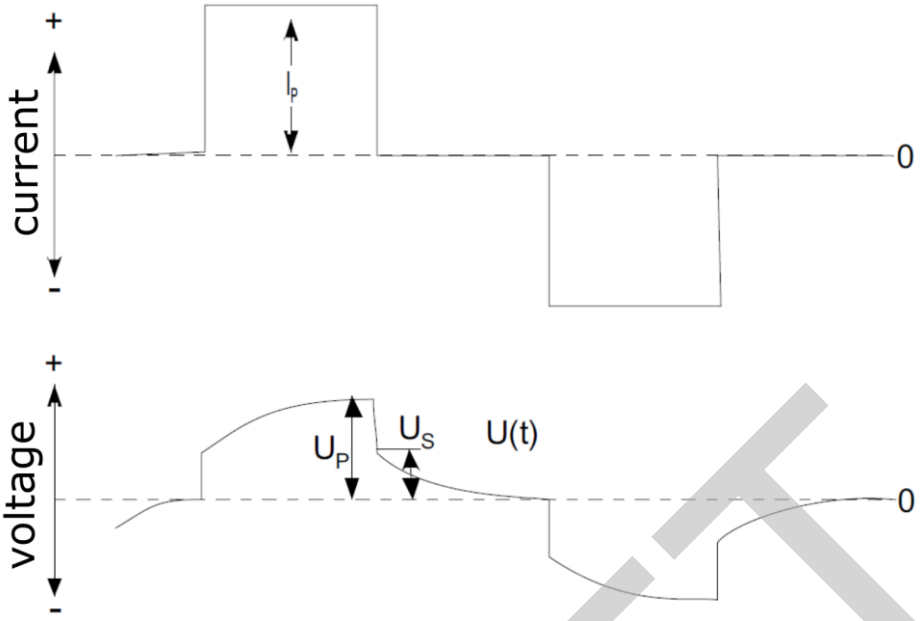

Figure 3 Theoretical full waveform potential for DCIP measurements with indication of parameters important for the data evaluation.

IP data can be measured with the same equipment and simultaneously with resistivity data, it is however much more challenging due to smaller measured signals.

2.3 Seismic refraction

In every seismic method an image of the subsurface will be obtained by the generation of elastic waves. Of the different types of seismic waves that exist, the most important ones are the p-wave (longitudinal of compression wave) and the s-wave (shear or transverse wave). The particle motion of the p-wave is in the direction of propagation. They cause volume and shape changes. The s-wave is polarised perpendicular to the direction of propagation and causes only shape changes. Both types are coupled, dividing the seismic energy partly in p-waves and s-waves. They are converted from one to the other type when reflected or refracted. In general, the velocity of seismic waves depends on elastic parameters and the density of the media, which makes it sensitive to lithological changes. Principally, p-waves have a higher velocity compared with s-waves in the same medium and s-waves cannot propagate in fluids, as no shear stress is supported. While propagating through the subsurface, seismic waves are reflected, refracted or diffracted, if a contrast in the elastic properties appears, such as at boundaries between different rock masses. Thus, conclusion about the lithological structure of the subsurface can be drawn from seismic surveys. Different sources for the excitation of elastic waves can be used. The most common ones are a sledgehammer, vibrator of explosives. All seismic methods are governed by Snell's law given in equation 1, which describes the relationship between the angles of incidence and refraction, when a seismic wave passes through a boundary.

$$\frac{\sin \alpha_1}{\sin \alpha_2} = \frac{v_1}{v_2} \qquad (3)$$

It states that the ratio of the sines of the angles between an incidence and refraction equals the ratio of the seismic velocities of the two media. Figure 2 is a schematic sketch of the principle of Snell's law that shows an interface between two layers with their seismic velocities v_1 and v_2. The incident wave is refracted at the interface. Because $v_2 > v_1$, the angle towards the normal of the interface increases.

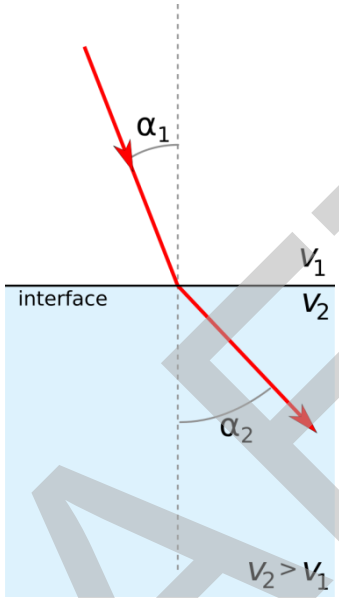

Figure 2: Behaviour of a seismic wave at an interface between layers with different acoustic properties

Basically, a seismic source generates elastic waves, which travel through the subsurface and are detected by sensors at the surface, respectively. Travel times of the waves can be estimated, which are used to obtain an image of seismic velocities of the subsurface. Spherical waves radiate from the source. Their energy is distributed over a sphere with the area $a = 4\pi r^2$, which results in a decay that is inverse proportional to the square of the distance. This decay is independent of the wave frequency. Due to the non-elastic behaviour of real material a part of the seismic energy is absorbed, which is frequency dependent.

A schematic sketch of expected travel times for a horizontal reflector is shown in Figure 3. An incident seismic wave splits up into a reflected and refracted wave at each boundary, at which the acoustic properties change.

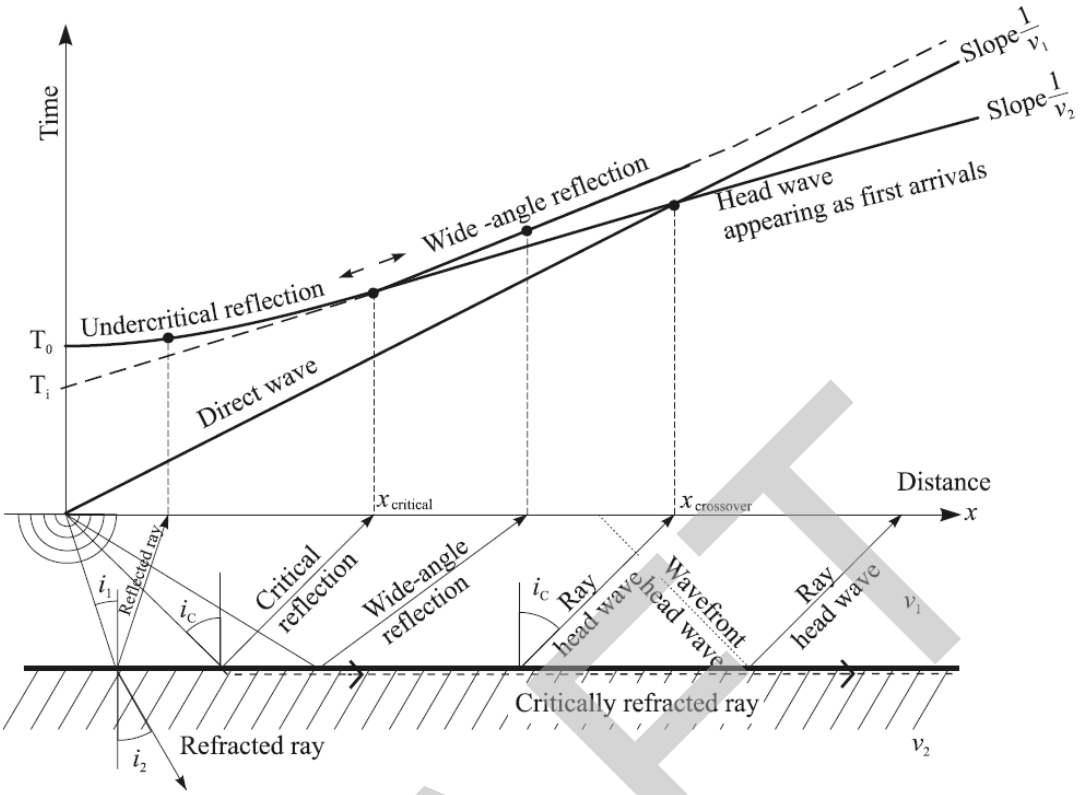

Figure 3: Schematic sketch of ray paths and travel times for direct and critical refracted waves (Knödel et al., 2007)

A critical refraction appears for a critical angle i_c between the incident wave and the normal of the boundary. In that case, the seismic wave propagates along the layer boundary in the lower layer. While propagating, secondary waves are transmitted as wave-fronts to the surface, which are called head waves. The relation between the travel time and the distance from the shot point is linear for the direct wave as well as for the head wave of the refraction, whereas a hyperbolic relation appears for a reflexion. Refraction seismic is an important near surface application, in which only the head waves are used. It requires an increasing seismic velocity with depth, otherwise no critical angles appear as the angle towards the normal of the interface decreases according to Snell's law. After the first arrivals have been identified and interpreted, the depth of interfaces, their dip and layer velocities can be estimated. Figure 4 shows a schematic sketch of a refraction seismic survey.

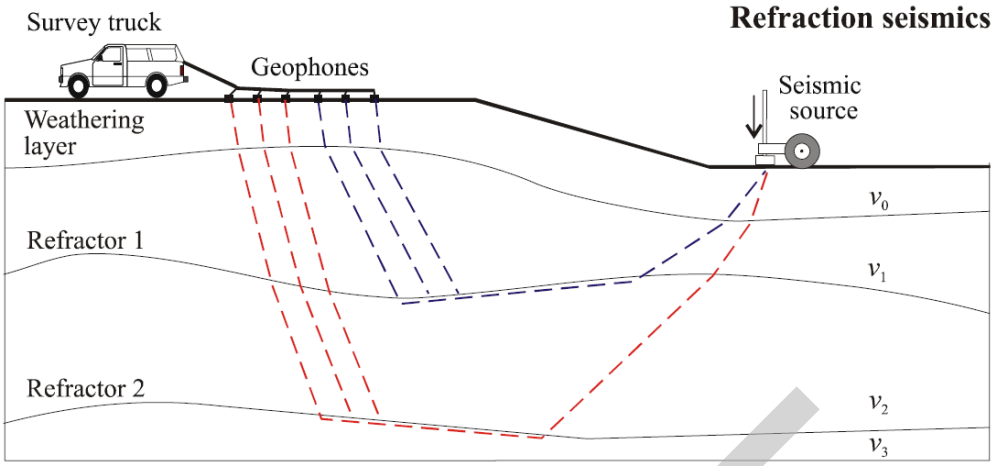

Figure 4: Schematic seismic refraction survey with refractions from two interfaces (Knödel et al. 2007).

2.4 Standard inverse modelling

Hypotheses of fundamental processes are developed on the base of observations, which can be translated into a simpler mathematical form used for its description. The process of liking for a solution of a special mathematical problem is called modelling. By varying model parameters, a set of synthetic data can be found that fit observations. Modelling can be schematically expressed by:

$$\mathbf{d}^{\mathrm{syn}} = \mathbf{F}(\mathbf{m}) \qquad (4)$$

whereas $\mathbf{d}^{\mathrm{syn}}$ is a vector of synthetic data with $\mathbf{d} = (d_1, d_2, \ldots, d_N)^T$, $\mathbf{m}$ a vector of model parameters with $\mathbf{m} = (m_1, m_2, \ldots, m_M)^T$ and $\mathbf{F}$ is a mathematical mapping or forward operator. It describes a non-linear problem, in which the synthetic data depends from the model. For linear problems, the equation above converts into the simple matrix multiplication $\mathbf{d}^{\mathrm{syn}} = \mathbf{Fm}$. Here a distribution of model parameter is given, from which synthetic data are predicted. The problem can be handled the other way around, which means that a set of model parameter is sought that explains observed data the best and can be expressed by:

$$\mathbf{m}^{\mathrm{est}} = \mathbf{F}^{-1}(\mathbf{d}^{\mathrm{obs}}) \qquad (5)$$

Here, $\mathbf{d}^{\mathrm{obs}}$ are observed data and $\mathbf{m}^{\mathbf{est}}$ are the estimated model parameter. This is called inverse modelling and describes in general the search of an optimal set of model parameter that explains the given set of observed data. The conversion of a geophysical data set into a spatial distribution of a parameter is the main objective of inverse modelling. If an optimal set of model parameters is sought, the residuum **e** between synthetic and observed data is minimized.

$$\mathbf{e} = \mathbf{d}^{\mathrm{obs}} - \mathbf{d}^{\mathrm{syn}} \qquad (6)$$

Several methods exist for minimizing **e**. The most common one is the least-squares method. Often data errors are taken into account, resulting in the objective function:

$$\Phi_d(\mathbf{m}) = \sum_{\mathrm{i}=1}^{\mathrm{N}} \left| \frac{\mathrm{d_i} - \mathrm{F_i}(\mathbf{m})}{\epsilon_\mathrm{i}} \right|^2 \qquad (7)$$

For the comparison of different data sets, the χ^2-value ($\Phi_d(\mathbf{m})/N$) has proven to be useful, as it is independent of the data amount. The inversion of non-linear problems is an iterative process with a starting model $\mathbf{m^0}$, which is modified by model updates $\Delta\mathbf{m}$ until the forward response f($\mathbf{m}$) fits the observed data to an acceptable degree. A new model is calculated in each iteration step n with $\mathbf{m}^{n+1}=\mathbf{m}^n + \Delta\mathbf{m}^n$. Most geophysical cases represent ill-posed problems, in which no unique and stable solution is defined. Therefore, we ensure a unique solution by introducing the additional regularisation term Φ_m in the objective function, which reduces the variability (roughness) of the model parameter and leads to smoother models. In general, the objective function that has to be minimized reads:

$$\begin{aligned} \Phi &= \Phi_d + \lambda\Phi_m \qquad (8) \\ &= \sum_{\mathrm{i}=1}^{\mathrm{N}} \left| \frac{\mathrm{d_i} - \mathrm{F_i}(\mathbf{m})}{\epsilon_\mathrm{i}} \right|^2 + \lambda \left\| \mathbf{C}(\mathbf{m} - \mathbf{m}^0) \right\|_2^2. \end{aligned}$$

The matrix $\mathbf{C}$ holds the derivatives and $\mathbf{m}^0$ is the reference model. The regularization parameter λ is chosen such that the data d_i of fitted by the forward responses f_i statistically within their error levels (χ^2=1). Additional model constrains can be incorporated in the object function by extending Φ_m to the weighted model functional

$$\Phi_m = \|\boldsymbol{W}_c \boldsymbol{C}\boldsymbol{m}\|_2^2 \qquad (9)$$

The weighting matrix $\mathbf{W}_c$ is diagonal and contains the elements w_i^c, which are penalty factors for the different model cell boundaries. Very small values correspond to sharp boundaries.

2.5 Joint inverse modelling using structural coupling

The idea behind a joint inversion of data sets from different geophysical methods is to improve inverse modelling results by reducing the ambiguity of the different models thus obtaining a more reliable model of the subsurface. The used approach enables the exchange of structural information between different inversions. Incorporation of topography is possible due to unstructured meshes and other additional geometric information.

Single geophysical methods often lead to non-unique results and ambiguous interpretation. For example, a decrease in electrical resistivity is explainable by a higher salt concentration in the water or by a change in lithology from resistive sand to more conductive sandy clay. Another very similar example is that it might not be possible separate a saltwater contaminated sand from a clay formation due to their similar resistivity. Due to a limited amount of data collected, the geophysical inversion also suffers a non-uniqueness. As shown above. Due to the smoothing sharp boundaries are not well imaged. The structurally coupled joint inversion of two geophysical methods is used to reduce the effects of smoothing constraints by identifying common structures between the two fitted models (Günther et al. 2006). The schematic sketch in Figure 5 shows how the inversion of one method is influenced by the other.

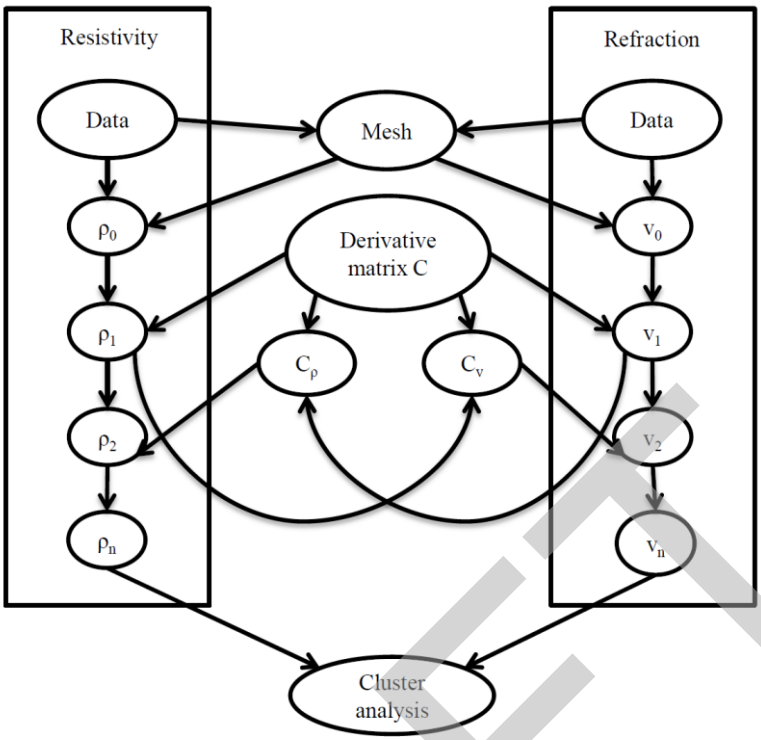

Figure 5: Scheme of the coupled inversion approach, in which one inversion influences the roughness C of the other, (Günther et al. 2006)

2.6 Cluster analysis

The aim of cluster analysis is to analyse a set of data, divide the data into subgroups that are referred to as clusters. Imagine a data-set that consists of electrical resistivities and P-wave velocities from refraction seismics, see Figure 6. The general idea is that data points could be automatically separated by the use of a clustering algorithm. Clustering is an unsupervised task; this makes it very different from supervised tasks such as classification and regression, where there is a specific target value. There is actually no need for a target value other than the number of clusters. Just as there is different ways for a human to learn, there are different clustering algorithms that can be implemented on a computer. We have chosen the k-means algorithm as it is easy to understand and implement. A trial and error procedure for trying out other algorithms that could be better suited for geophysical is what should be employed.

The k-means algorithm may be applied on points in a d-dimensional vector space; the algorithm clusters a set of d-dimensional vectors, denoted D. $D = \{\boldsymbol{x_i} | i = 1, \dots, N\}$, and $x_i \in R^d$ denotes the i:th object of data point. K-means divides the D into k number of clusters. The books are kept by assigning each point a cluster ID and the points that are sharing ID's are hence in the same cluster. The number of clusters can be found by trial and error combined with the prior knowledge of the data-set. Every cluster is represented by one single point, referred to as the cluster centre. These cluster representatives are denoted by the set $C = \{\boldsymbol{c_j} | j = 1, \dots, k\}$. The k-means algorithm minimizes the nonnegative cost function:

$$Cost = \sum_{i=1}^{N} \left(argmin \|\boldsymbol{x_i} - \boldsymbol{c_j}\|_2^2 \right) \quad (10)$$

And this this implies that the algorithm is seeking to minimize the total squared Euclidian distance between each point $\boldsymbol{x_i}$ and the cluster centre $\boldsymbol{c_j}$ closest to it. The cost function that is beeing minimized is referred to as the objective function of the k-means algorithm.

Figure 6: K-means clustering on artificial data, adapted from Joydeep and Alexander (2009).

The k-means algorithm work in two iterative and separate step:

1. Assigning data to the centre that is closest to it.
2. Relocation of the cluster centre so that it is in the middle of its cluster.

3 Examples

3.1 Äspö Hard Rock Laboratory

The Äspö field study consists of collocated ERT and seismic refraction measurements along a single line crossing over both land and brackish water. In order to increase the reliability of the results the combined analysis of the methods will be investigated, as described in the method chapter, through joint inversion and joint interpretation with cluster analysis. The fieldwork was performed in the spring of 2015. The ERT measurements were performed in cooperation with TRUST 2.1 and the land seismic measurements were performed in cooperation with TRUST 2.2. In addition, the survey boat used for the seismic work was also used for collecting RMT on the water together with TRUST 2.2.

The Äspö HRL was built by the Swedish Nuclear Fuel and Waste Management Company for research into deep repository of spent nuclear fuel (Rhén et al. 1997). It compromises of an access tunnel reaching 460 m in depth and spanning 3600m, which was constructed after extensive site investigations of the area. As such, it presents itself as a study area with comprehensive background on geological and hydrological conditions of the deep subsurface. This extensive reference data together with the geological setting, that in many ways delivers typically Scandinavian challenges, constituted the main reasons for choosing Äspö HRL as a study site.

The first site investigations for the Äspö HRL started in 1986. Measurements were made in different scales using airborne EM, gravimetric, petrophysical measurements and a mapping of solid rocks and analyses of main structures, such as fracture patterns on a regional scale. Geophysical data indicated an orthogonal regional pattern consisting of features trending N-S and E-W. Detailed ground based observations by seismics, VLF and magnetics showed that most features are very narrow indications less than 10 m wide, associated with increased fracturing, (Wikbert et al. 1991). The mapping of fractures at outcrops showed that they exceed 0.5 m with a surface area from 30 to 200 m^2 with main dips of 70° to 90°. The direction of the predominant fractures is E-W, N60°W, N5°E and N75°E. Concerning the filling, epidote and quartz have been formed in deeper processes. Calcite, which may be formed by hydrothermal processes can be used as an indicator for water paths in the rock, (Wikbert et al. 1991). They found out that fractures in N-S and E-W directions could most likely conduct water. According to Stanfors et al. 1999 the fractures identified as NE-1, NE-2 and NE-4 are of

main interest, with NE-1 comprised of three branches, which are intensely fractured and hydraulically conductive.

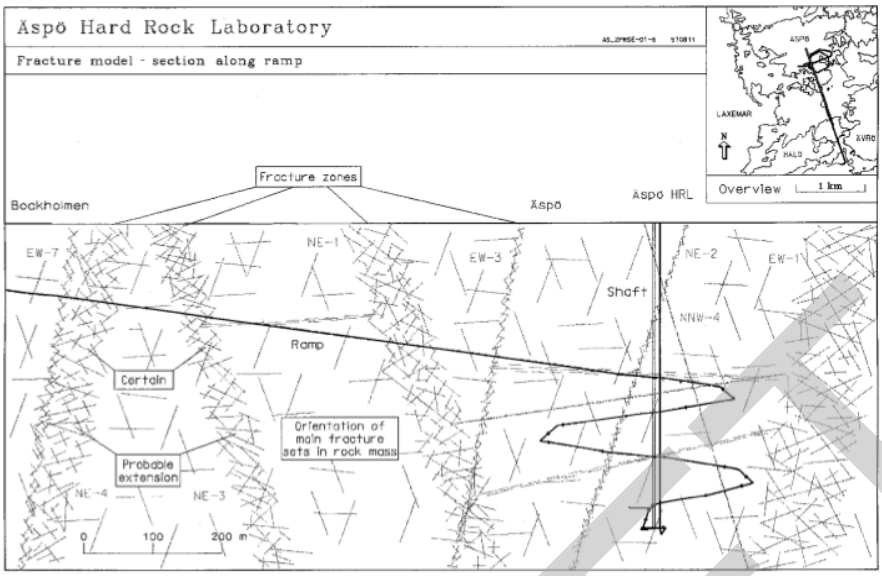

Figure 7: Fracture zones at Äspö HRL (Stanfors et al. 1999)

The objective of the Äspö HRL survey is to locate fracture zones at Äspö HRL at the tunnel part between Hålö and Äspö. As seen in Figure 7 it is mainly fractures NE-1, NE-3, NE-4 an EW-7 that are in focus.

The surveys were conducted in April 2015. For the geophysical surveys the ERT and seismic profile was oriented in north-south direction. Collocated sensor positions for ERT and seismic were used. Electrodes were placed on-shore and underwater with a 5 m spacing along a 780 m profile. The seismic refraction data collected on the seabed used a streamer with 91 hydrophones with 5m spacing and a total length of 450 m. The topography of the seabed was mapped with a multibeam echo sounder. Small explosives, approximately 0.5 m above the seabed, were used for the excitation of seismic waves. The recorded data were processed with Rayfract refraction tomography software. In addition, the explosive shots from the seismic measurements on the seabed was also recorded on land by the TRUST 2.2 team. This data will be available to TRUST 4.2 in the spring 2016, and will then provide an opportunity to model land and marine data simultaneously.

Both the seismic and the ERT measurements provide some challenges due to poor ground conditions at the test site. On land, large contact impedances demand high currents in order to obtain measurable signals for ERT. And for the southern part of the seismic line high attenuation of the seismic signals, due to gas filled sediments, made it difficult to determine first arrivals.

The seismic data fit is shown in Figure 8. Travel times for larger offsets are not aligned linearly as expected for refracted waves, which is probably caused by undulations of the layer boundary. Larger offsets for the shot points 5 and 6 (purple and yellow) exhibit larger misfits compared to other shot points and have a steeper slope. An explanation could be a poor data

quality that makes it difficult to determine first arrivals. Early times of all shots could be fitted well.

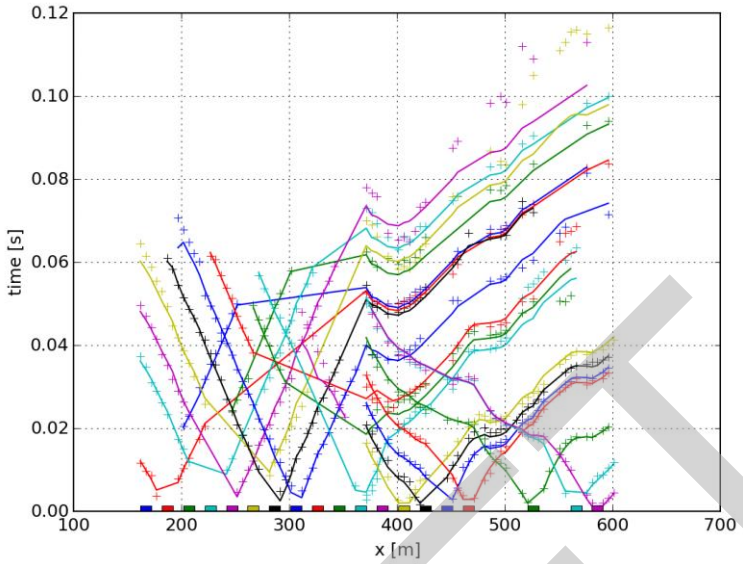

Figure 8: Raw data (marks) and the forward response (continuous lines) of the data fit from Äspö HRL. The shot points are marked with rectangles.

The inverse modelling result of the marine seismic data is shown in Figure 9. A low velocity zone appears at shallow parts of the model, which reaches depth of about 60 m between 200 – 400 m. A quite thin transition zone towards a high velocity zone with v ca. 6000 m/s follows. The low velocity zone is interpreted as sediments. A large amount of gas bubbles appeared after the explosions and indicate that the sediments could be partially filled with gas. The high velocity zone corresponds with the bedrock. Lower velocities appear within the bedrock, which are probably caused by fracture zones.

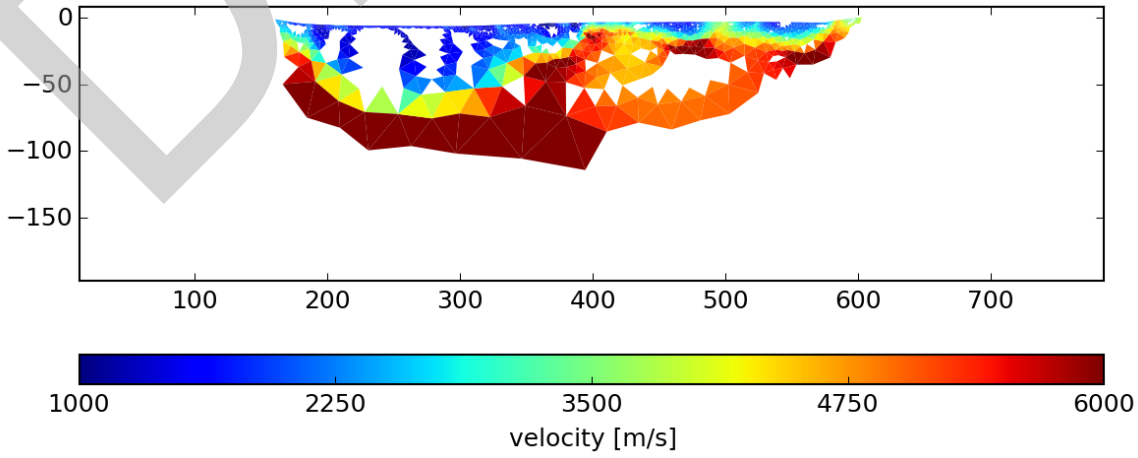

Figure 9: Inverse modelling result of seismic data from Äspö HRL. Model parts with a low coverage are faded out

The ERT result (Figure 10) shows a low resistive zone blow the lake. At approximately 200-300m this zone extended deeper. This is in agreement with seismic result. A low velocity and low resistivity towards depth indicate a zone with thick sedimentary deposits. In general, the resistivity result indicates a thicker layer of low resistivity compared to the low velocity zones. By setting the threshold for the low resistivity zone to approx. 32 Ωm, a maximum depth towards the bedrock of about 60 m is reached. A low resistive zone extends towards north (right in Figure 10) to x > 600 m. This could correspond to the known fracture zone NE1, but could also be explained by 3D effects from the lake that continues parallel to the ERT just a few metres offline from the ERT profile. This can only be avoided by 3D survey.

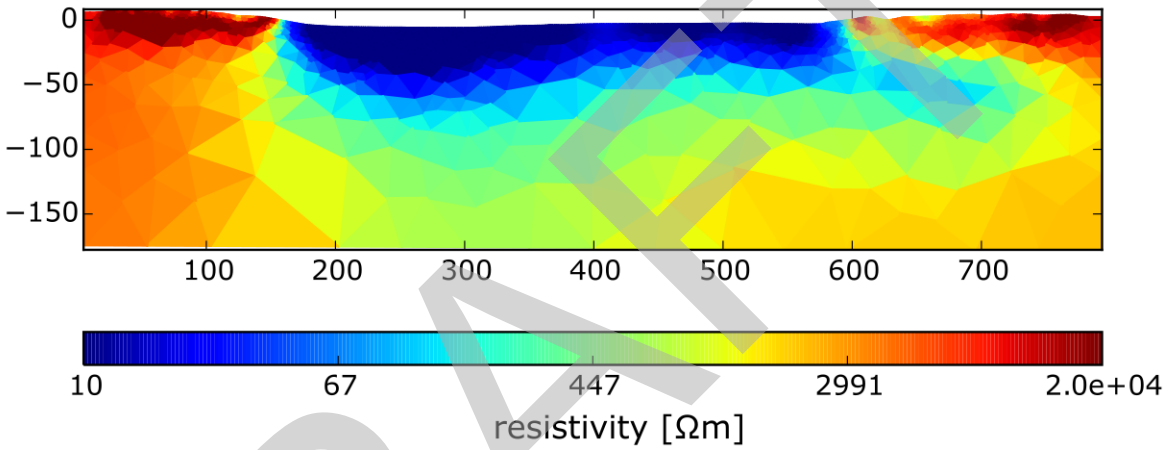

Figure 10: Inverse modelling result of the ERT survey from Äspö HRL.

The interface towards the bedrock below the sedimentary deposits is not exactly resolvable. The bedrock appears with a lower resistivity in this part, which might be a result of the smoothness constraints, as an un-fractured bedrock should exhibit larger resistivities.

In order to improve the results of the inverse modelling, i.e. reduce the transitions zones in both results, a joint inverse modelling of the ERT and seismic data set was performed using the coupling approach described above. The first two iterations were done separately. The coupling was applied starting with the third iteration step. For comparison, the same regularisation parameter as for the separated inversions were used for ERT and seismic. Generally, they are adjusted such that both data sets can be fitted within their errors, i.e. $\chi^2 = 1$. The result of the joint inverse modelling is shown in Figure 11.

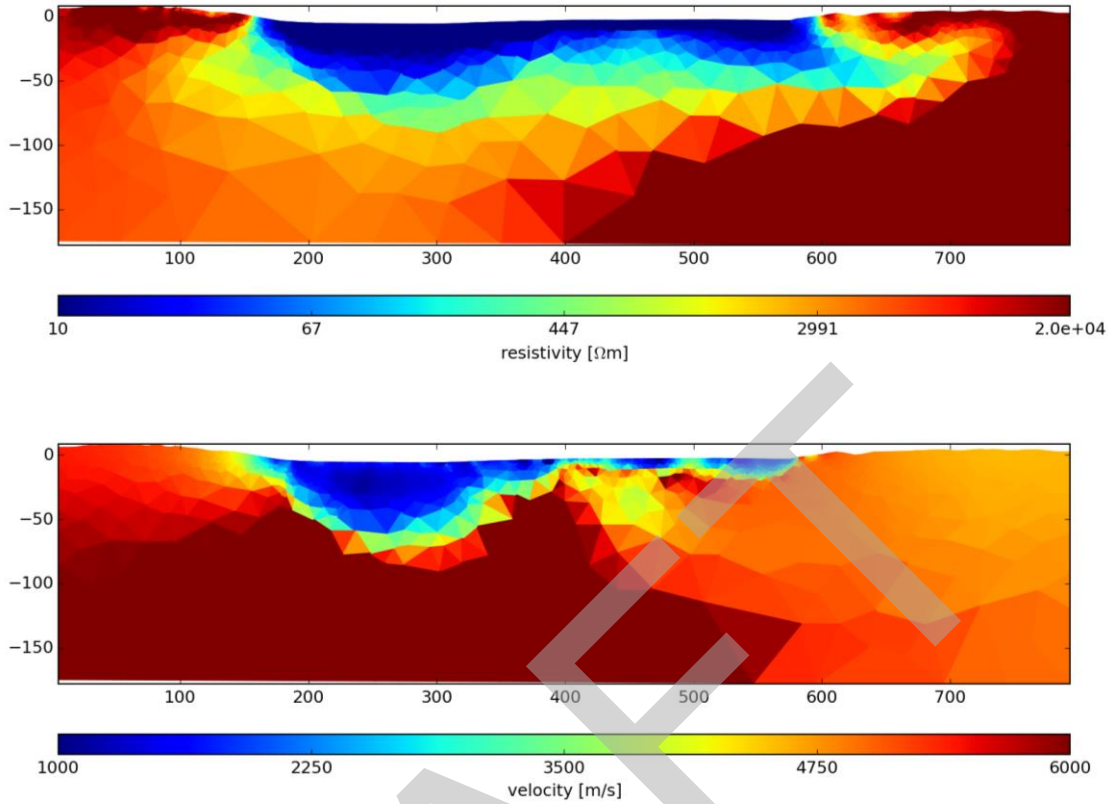

Figure 11: Result of joint inverse modelling of the ERT (top) and seismic (bottom) data from Äspö HRL

The upper picture of Figure 11 shows the ERT result and the bottom picture the seismic result. Due to the coupling, both models could be improved. Compared to the separated inversions, the low resistive zone, which correspond to the sedimentary deposits, now appears thinner than before. Higher resistivities appear below the sediments. The interface between the bedrock and the sediments appears sharper in the seismic result as well. While interpreting the data, it has to be taken into account that 3D effects might influence the result, which cannot be taken into account in a 2D inversion. Lower resistivities still appear between 200m<x<300m, while the seismic result shows the highest velocities. Up to this point, this is very difficult to interpret, due to a low coverage in this model part. It is planned to merge the land seismic data from TRUST 2.2 with this data set, which can possibly lead to a better coverage for this part and thus lead higher investigation depth. For pre-processing the results of the inverse modelling, a cluster analysis was done, which is shown in Figure 12. For calculating the clusters, only model parts with a sufficient coverage should be taken into account. Only resistivities and velocities of model parts where the coverage exceeds 0.001 were used as an input for the cluster analysis. The blue coloured model domain includes only low resistivities and seismic velocities, which is interpreted as sedimentary deposits. The bedrock, which exhibits high resistivities and velocities is marked red. The green part is an intermediate zone, in which the interface between the sediments and the bedrock might be located.

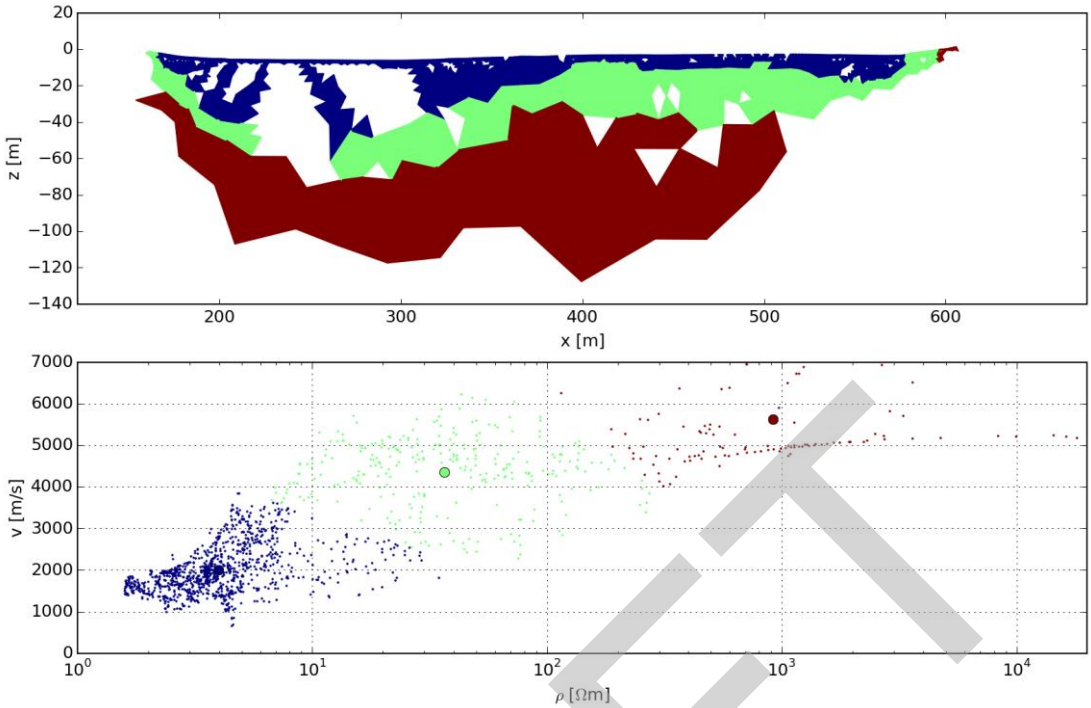

Figure 12: Result of the cluster analysis for the joint inversion result of Äspö using three clusters.

3.2 E16 Norway

Seismic methods and seismic refraction in particular is a standardized tool for tunneling site investigations in Norway (Rønning et al. 2009). Seismic refraction has the ability to detect fracture zones, aid in the assessment of thickness of these zones and yield a specific seismic velocity for the investigated bedrock. The seismic velocity can then be used to qualitatively evaluate the bedrock.

There are basically two main approaches to the evaluation of seismic refraction data. Either using layer models and trying to fit the data to these models or using a tomographical approach. The advantage of using the tomographical approach is the possibility of detecting fracture zones with a limited extent in relation to the survey profile. A difficulty that appears in regions where glaciation has effectively scrapped the weathering zone clean is that there is a difficulty in transferring energy into the bedrock; this problem is often pronounced in most parts of Norway. This implies that it will be most difficult to attain information from within the bedrock, meaning that the dip and depth of fractured zones will be unknown.

ERT (electrical resistivity tomography) can be used to locate fracture zones within the bedrock, yielding further information such as zone thickness and dip (Rønning et al. 2009; Reiser et al. 2009).

The Norwegian road administration is planning a new 8.5 km long stretch of four lane highway (E16) from Bjørum to Skaret. The project is complex from the point that 4.2 km of the total stretch is planned to be tunnelled, and the need for deep bedrock quality assessment is

pressing. The selected stretch for this particular analysis is only about 700 meters long and meant to act as a test stretch.

The site is located in the S-E part of Norway, as described in Figure 13. Rambøll conducted the field survey and wrote a report (Rambøll 2012) for the Norwegian geological survey and GeoVita AS. The results from the survey were interpreted and used to update an expected geological section that was first created by using the geological maps and surface mapping by an experienced local geologist.

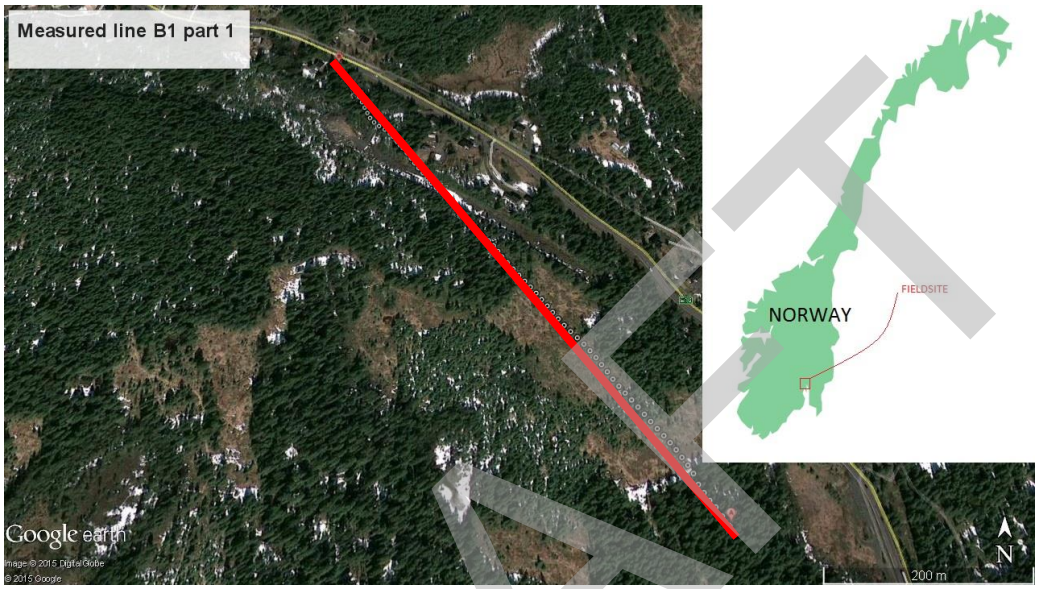

Figure 13: Location of the conducted ERT and refraction seismic profile (B1 line). The regional location is given in the inlet.

The field site is situated in within the Oslo Rift. The rift can be subdivided into three major graben structures from the north, the Askershus Graben (AG), the Vestfold Graben (VG) and the Skagerrak Graben (SG). During Perm, the rift was experiencing volcanic activity that peaked 295-285 million years ago. Volcanic deposits of porphyry and basalt are predominant and there are volcanic rock dikes over 40 meters wide. The volcanic layers in the area are surrounded by faults and syenite dikes. Glacial events have removed large amounts of heavily weathered bedrock and replaced it with thin till layers.

The ERT results are presented in Figure 14. A high (1250-3980 Ωm) resistivity strip can be seen close to the surface. The underlying layer shows two vertical anomalies at 300 and 450 meters respectively. The apparent horizontal stratification pattern suggests horizontal geological structures. These patterns coincide with expected volcanic structures. The vertical high (1250-3980 Ωm) resistivity band at 300 meters coincides with dolerite findings at the surface, indicating a vertical dyke.

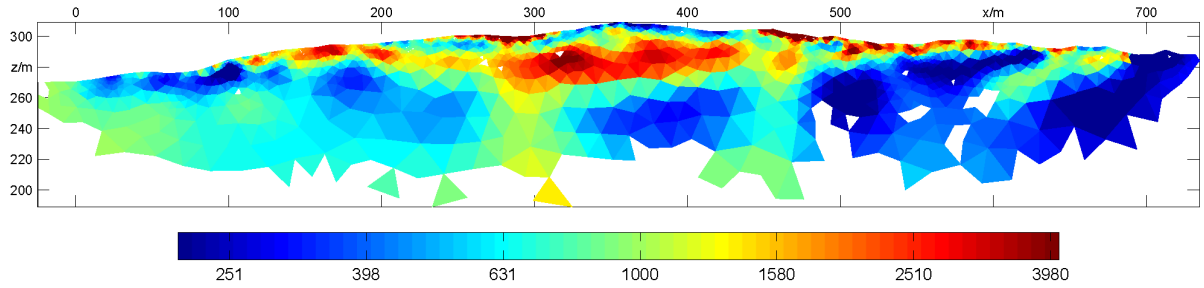

Figure 14: Inversion result of the resistivity profile [Ohm-m]

The inverted velocity section in Figure 15 shows one or two low (1000-3500 m/s) velocity layers. These layers are on top of a high (3501-5200 m/s) velocity layer, divided into three separate parts at 100 and 450 meters. The outer part of this layer contains ever higher velocities (4500-5200 m/s). The possible dolerite indicated in the resistivity profile could be present at 300 meters, indicated by a high (4500-5200 m/s) velocity zone. There is a low (3500-4000 m/s) velocity part just left of this, possibly indicating some weathering adjacent to the dyke.

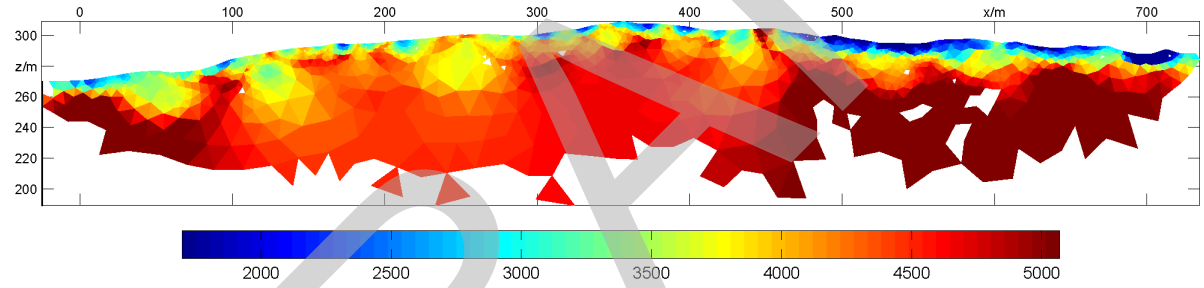

Figure 15: Inversion result of the refraction seismic survey [m/s]

The co-interpreted section in Figure 16 is based on joint inversion of the two data sets followed by cluster analysis. At 300 meters, there is visible diabase at the surface; this diabase zone could be in coherence with the blue zone. The dominating turquoise zone is more difficult to interpret; it probably consists of less weathered bedrock. The green and yellow near surface outcrop zones are probably diabase and volcanic rocks in different stages of weathering.

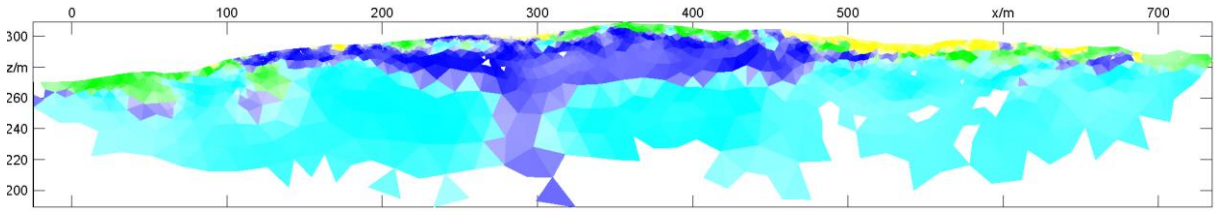

Figure 16, Co-interpreted results, 4 clusters

The ERT results exhibit a model section with structural information throughout the depth of the sections, with zones of lower resistivities indicated to large depths. For the seismic refraction, on the other hand, there is no indication of changes in velocity below approximately 30 metres depth.

The automatically interpreted section can be easier to interpret and helps the interpreter to find the common patterns that are subtler in the separate profiles. The evidence of a vertical volcanic dike becomes very clear in this profile.

Following up the geophysics with a drilling campaign is a natural step. The drilling campaign may be designed by using the results from the geophysical and thereby making the most of the drillings. A future outlook is to include drill-data and revise model using drill-data. This facilitates a very detailed assessment of rock quality and fracture zone extension.

4 Summary and conclusions

In order to test integrated use of inversion approaches and analysis, field surveys were conducted. Separated and joint inversion algorithms were used to fit the field data in an attempt to obtain reliable results. In order to facilitate interpretation of geophysical parameter distributions like electrical resistivities and seismic velocities, cluster analysis was applied to the inversion results. Field surveys conducted at Äspö HRL and in Norway are presented.

Results at Äspö showed that the sharp interface between the sedimentary deposits and the bedrock could not be determined correctly by ERT. Even the seismic result exhibit a larger transition zone between low and high velocities. The joint inversion of both data sets could improve the results by sharpening the interfaces towards the expected bedrock. In addition, the cluster analysis could identify 3 subdomains with similar rock properties each, separating the sedimentary deposits from the bedrock. The third cluster, which shows a thin transition zone for seismic and ERT marks the depth range, in which the interface between the sediments and the bedrock can be assumed.

The second example, based on field surveys conducted for a new stretch of E16 in Norway, shows that the cluster analysis can clearly identify a dike-like structure, which corresponds possibly to a more weathered or fractured zone within the bedrock.

The results are promising and will be used for further evaluation of the field data sets against available reference data, and for further development and refinement of the interpretation methodology.

5 Outlook

The developed interpretation algorithms will be tested against all the acquired data, incorporating the IP data as well as resistivity and refraction seismics. This applies to the data acquired at ESS in Lund, Kv Färgaren in Kristianstad, the Varberg tunnel, Äspö HRL, Önneslöv-Dalby, Stockholm Bypass at Lambarfjärden and Östlig förbindelse. The results of the tests used for further development and refinement of algorithms. Further analysis of the Äspö field case are planned, including the land seismic data collected by Uppsala University.

Field measurements in boreholes are planned, which can be done either with different geophysical borehole logs for information to detail the correlation, either by measuring between the electrodes and seismic sensors in different boreholes or between boreholes and on land.

The development of methodology for estimation of rock technical parameters of importance for tunneling will be included, i.e. water leakage and rock stability, based on geophysical data combined with other data that is normally available in this type of project. The intention is to test the model against data from actual underground projects, but there remains considerable work to develop, analyze and quality assure the necessary reference data for this.

6 References

Auken, E., & Christiansen, A. V. (2004). Layered and laterally constrained 2D inversion of resistivity data. *Geophysics*, *69*(3), 752–761. doi:10.1190/1.1759461

Cavinato, G. P., Di Luzio, E., Moscatelli, M., Vallone, R., Averardi, M., Valente, A., & Papale, S. (2006). The new Col di Tenda tunnel between Italy and France: Integrated geological investigations and geophysical prospections for preliminary studies on the Italian side. *Engineering Geology*, *88*(1), 90–109.

Dahlin, T. (2001) The development of electrical imaging techniques, Computers and Geosciences, 27(9), 1019-1029.

Dahlin, T., Bjelm, L., & Svensson, C. (1999). Use of electrical imaging in site investigations for a railway tunnel through the Hallandsas Horst, Sweden. *Quarterly Journal of Engineering Geology and Hydrogeology*, *32*, 163–172.

Danielsen, B. E. (2007). The applicability of geoelectrical imaging as a tool for construction in rock. *Quarterly Journal of Engineering Geology*, *32*, 163–172.

Di, Q., & Wang, M. (2010). Determining areas of leakage in the Da Ye Dam using multi-electrode resistivity. *Bulletin of Engineering Geology and the Environment*, *69*(1), 105–109.

Dietrich, P., & Tronicke, J. (2009). Integrated analysis and interpretation of cross-hole P-and S-wave tomograms: a case study. *Near Surface Geophysics*, *7*(2), 101–109.

Gallardo, L. A., & Meju, M. A. (2004). Joint two-dimensional DC resistivity and seismic travel time inversion with cross-gradients constraints. *Journal of Geophysical Research*, *109*(B3), B03311.

Günther, T., Bentley, L. & Hirsch, M. (2006) A new joint inversion algorithm applied to the interpretation of dc resistivity and refraction data. In Proceedings of XVI International Conference on Computational Methods in Water Resources.

Haber, E., & Oldenburg, D. (1997). Joint inversion: a structural approach. *Inverse Problems*, *13*(1), 63.

Infante, V. et al., (2010) Lithological classification assisted by the joint inversion of electrical and seismic data at a control site in northeast Mexico. Journal of Applied Geophysics, 70(2), pp.93–102.

Joydeep, G., & Alexander, L. (2009). K-Means. In *The Top Ten Algorithms in Data Mining* (pp. 21–35). Chapman and Hall/CRC.

Juhojuntti, N., & Kamm, J. (2015). Joint inversion of seismic refraction and resistivity data using layered models — Applications to groundwater investigation. *Geophysics*, *80*(1), EN43–EN55. doi:10.1190/geo2013-0476.1

Knödel, K., Lange, G. & Voigt, H.J. (2007) Environmental Geology – Handbook of Field Methods and Case Studies. Chapter 4.6 Seismic Methods. Schuck, A. & Lange G. *Springer*, 337 – 402.

Linde, N., Tryggvason, A., Peterson, J. E., & Hubbard, S. S. (2008). Joint inversion of crosshole radar and seismic traveltimes acquired at the South Oyster Bacterial Transport Site. *Geophysics*, *73*(4), G29–G37.

Lines, L. R., Schultz, A. K., & Treitel, S. (1988). Cooperative inversion of geophysical data. *Geophysics*, *53*(1), 8–20.

Nijland, W., van der Meijde, M., Addink, E.A., de Jong, S.M., 2010. Detection of soil moisture and vegetation water abstraction in a Mediterranean natural area using electrical resistivity tomography. *CATENA* 81, 209–216.

Nur, A., Mavko, G., Dvorkin, J., & Galmudi, D. (1998). Critical porosity: A key to relating physical properties to porosity in rocks. *The Leading Edge*, *17*(3), 357–362.

Paasche, H., Tronicke, J., Holliger, K., Green, A. G., & Maurer, H. (2006). Integration of diverse physical-property models: Subsurface zonation and petrophysical parameter estimation based on fuzzy c-means cluster analyses. *Geophysics*, *71*(3), H33–H44.

Rambøll, (2012) Grundundersøgelser for ny e16 mellem bjørum og skaret, Report.

Reiser, F. et al. (2009) Resistivity Modelling of Fracture Zones and Horizontal Layers in Bedrock. NGU rapport 2009. 070., p. 120 sider.

Rønning, J.S. et al. (2009) NGU Rapport 2009.064 Resistivitetsmålinger og retolking av seismikk langs E6 og Dovrebanen ved Mjøsa.,

Sasaki, Y. (1989). Two-dimensional joint inversion of magnetotelluric and dipole-dipole resistivity data. *Geophysics*, *54*(2), 254–262.

Seigel, H.O. (1959) Mathematical formulation and type curves for induced polarization. *Geophysics*, 24, 547–565.

Tronicke, J., Holliger, K., Barrash, W., & Knoll, M. D. (2004). Multivariate analysis of cross-hole georadar velocity and attenuation tomograms for aquifer zonation. *Water Resources Research*, *40*(1).

Tryggvason, A., & Flóvenz, Ó. G. (2002). Three-dimensional imaging of the P-and S-wave velocity structure and earthquake locations beneath Southwest Iceland. *Geophysical Journal International*, *151*(3), 848–866.

Vozoff, K., & Jupp, D. L. B. (1975). Joint inversion of geophysical data. *Geophysical Journal of the Royal Astronomical Society*, *42*(3), 977–991.

Wikbert, P, Gustafsson, G, Rhen, I. and Stanfors, R. (1991). *Äspö Hard Rock Laboratory. Evaluation and conceptual modelling based on the pre-investigations 1986-1990.* Technical Report, SKB (Swedish Nuclear Fuel and Waste Management Company), 91-22.

Appendices

Paper 1

Hellman K, Wennermark M, Günther T, Dahlin T & Rücker C (in revision after review) Structurally coupled inversion of ERT and refraction seismic data combined with cluster-based model integration, Geophysics.

Paper 2

Ronczka M, Wisén R, Dahlin T & Wennermark M (manuscript to be submitted) ERT and seismic refraction tomography test at Äspö Hard Rock Laboratory. (Engineering Geology)

Structurally coupled inversion of ERT and refraction seismic data combined with cluster-based model integration

Kristofer Hellman*, Marcus Wennermark*, Thomas Günther†, Torleif Dahlin* and Carsten Rücker‡

*Department of Engineering Geology
Lund University
Box 118
SE-221 00 Lund
Sweden
†Leibniz Institute for Applied Geophysics
Stilleweg 2
D-30655 Hannover
Germany
‡Technische Universität Berlin
Ernst-Reuter-Platz 1
D-10587 Berlin
Germany

ABSTRACT

Electrical resistivity tomography (ERT) and refraction seismics are among the most frequently used geophysical methods for site-investigations and the combined results can be very helpful to fill in the gaps between the point measurements made by traditional geotechnical methods such as CPT, core-drilling and geophysical borehole logging. The interpretation of the results from a geophysical investigation constituting a single method often yields ambiguous results. Hence, an approach utilizing multiple techniques is often necessary. To facilitate interpretation of such a combined dataset, we propose a more controlled and objective approach and present a method for a structurally coupled inversion of 2D electrical resistivity and refraction seismic data using unstructured meshes. K-means clustering is used to automate the interpretation. Two synthetic examples are used to demonstrate the method, and a field-data example is included to show the applicability in real-world situations. The inversion results for the field example in comparison with in-situ methods shows that a common lithological pattern is apparent. The methodology can be used as a tool for better data interpretation and for obtaining a more understandable and complete picture of the combined geophysical results.

INTRODUCTION

Geophysical methods have proved valuable for the site investigations in large projects (e.g. Dahlin et al., 1999; Cavinato et al., 2006; Danielsen, 2010; Di and Wang, 2010). Especially the combined usage of Electrical Resistivity Tomography (ERT) and refraction seismic is a feasible method for site investigations in preparation for tunneling and road-building in Scandinavia (Dahlin et al., 1999). The underlying motivation for combining two methods

based on different physical properties is the possibility to decrease the inherent ambiguities of each method (Linder et al., 2010). Ambiguities with ERT could be, for example, failure to detect a low contrast resistivity boundary between a layer of shale and a layer of clay. In this case, seismic profiling could possibly detect this boundary due to a high contrast in seismic velocity. The joint inversion of two separate datasets may also assist in improving the overall resolution, creating models that are in better agreement with each other, thus assisting the interpretation (e.g., Gallardo and Meju, 2004).

The use of more than one geophysical dataset for geophysical inversion was first presented by Vozoff and Jupp (1975). This should ideally result in a single subsurface model that can explain the datasets used (Lines et al., 1988). Several methods to perform joint or cooperative inversions have been developed (e.g., Lines et al., 1988; Haber and Oldenburg, 1997; Bosch, 1999; Paasche and Tronicke, 2007; Gallardo and Meju, 2011). Using data from several geophysical methods for interpretation can be done in three main ways: i) joint interpretation using different datasets that are separately inverted ii) joint inversion of separate data sets, iii) constrained inversion, where separate datasets constrain each other (Doetsch et al., 2012) . The joint interpretation approach suffers from ambiguities inherent in the model parameters. However, statistical tools could provide a more objective method to analyse the data (e.g., Tronicke et al., 2004; Paasche et al., 2006; Bedrosian et al., 2007), this approach is applied here in the post-processing stage as described in the methodology of this paper. The question of what kind of results are sought is also a very important part of formulating the inverse problem. There is a possibility not only to look for major geophysical structures in the data and hence create high resolution models which can aid the interpreter in finding for example a ground water surface. The additional use of petrophysical links between a geophysical property such as a certain resistivity, empirically linked to a specific hydraulic property through Archie's law could also be possible outcome. The underlying hypothesis that motivates the combined usage of electrical and seismic data states that there is a correlation between electrical resistivity and seismic velocity in heterogeneous earth materials. This is due to the influence on both of these geophysical parameters from the pore structure of the materials. The relationship between the geophysical parameters and porosity has been presented by Archie (1942) for resistivity and Wyllie et al. (1956) for seismic wave velocity. Other authors presenting this relation are e.g. Meju et al. (2003).

The methodology that we employ is a mutually structurally coupled cooperative inversion approach. This means that the structural pattern in one model is used to guide the inversion of the other and vice versa. Structural coupled inversion goes back to Zhang and Morgan (1996) and Haber and Oldenburg (1997). They minimize, additionally to the individual objective functions, a measure of dissimilarity of the models. Another very popular method to do so is called cross-gradients (Gallardo and Meju, 2004) where model gradients are penalized only if they go into different directions. The method is originally designed for regular grids, but was later extended to unstructured meshes (Lelivre et al., 2012). Here we follow yet another approach (Günther and Rücker, 2006) that does not need an additional objective function but works through an interchange between the individual smoothness matrices. A similar approach with ERT and surface wave seismic data was demonstrated by Wisén and Christiansen (2005). After completing a structurally coupled inversion, one is left with two or more geophysical model sections; our idea is to use cluster analysis to further aid the interpretation of the combined geophysical data. The cluster analysis is utilized to create a unified, automatic, numerical interpretation of the surveyed profile. Using clustering algorithms to aid interpretation has been shown to be a step towards a more automated and less ambiguous interpretation (e.g., Tronicke et al., 2004; Paasche and Tronicke, 2007; Linder et al., 2010).

This article extends on the ideas presented in Günther and Rücker (2006) and Günther et al. (2010), extending them to a complete interpretive framework and using unstructured triangular meshes. There are two main benefits of using these meshes; 1) a more computationally efficient cell division with local refinement, and 2) the possibility to include, without further adaptations, surface topography.

In order to provide a basis for the validation of the method presented here, two separate synthetic geophysical scenarios have been created. All the modeling, data analysis and inversions carried out within the scope of this article were done with the help of software that is freely available to the scientific community (Rücker and Günther, 2015). Finally, a field case is presented that shows how the structurally coupled inversion can deal with real data.

METHODOLOGY

The methodology described consists of three major parts: 1) Numerical forward models for resistivity and refraction seismic data, used both in the inversion scheme and to model the forward response for synthetic models; 2) The inverse modeling scheme, for structurally coupled mutual inversion of resistivity and refraction seismic data; 3) k-means cluster analysis for a final presentation of major units.

Synthetic resistivity forward modeling

The governing partial differential equation relating the potential u as a result of current injection $\boldsymbol{j}$ and the conductivity σ reads:

$$\Delta \cdot (\sigma \nabla u) = -\nabla \cdot \boldsymbol{j} \text{ in } \Omega \subset \mathbb{R}^3 \quad (1)$$

Even though the resistivity distribution is two-dimensional, i.e. constant along y, the point source is inherently three-

dimensional. Therefore the potential u is transformed into wave-number domain and solved for a series of wave numbers k_y.

$$\Delta \cdot (\sigma \nabla u) - k_y^2 \sigma u = -1/2 \nabla \cdot \boldsymbol{j} \text{ in } \Omega \subset \mathbb{R}^3 \qquad (2)$$

We follow the suggestion of Kemna (2000) combining Gaussian quadrature and Laguerre point integration. The individual wavenumber equations are solved by Finite Elements on triangle grids

We make use of the secondary potential (SP) approach (Rücker et al., 2006), i.e. only the deviation from a homogeneous half-space is computed which allows much coarser meshes. According to Günther et al. (2006), once at the beginning of the inversion, the potentials for a conductivity $\sigma = 1\,\mathrm{S/m}$ are computed on a highly refined mesh. In the course of inversion, SP calculation can be done on a much coarser mesh which speeds up the procedure significantly.

Synthetic refraction seismic modeling

The forward problem is to simulate the ray propagation for a given slowness distribution $s(\mathbf{r})$ to predict the *first arrival* times using Dijkstras algorithm (Dijkstra, 1959). The total travel time is the integral over the ray path l

$$t = \int_l dt = \int_l \frac{dl}{v} = \int_l s dl \qquad (3)$$

The modeling domain is subdivided into M model cells, where each cell has a constant slowness, s_j. In this discrete form the integral can be expressed as the sum

$$t = \sum_{j=1}^{M} l_j s_j \qquad (4)$$

where l_j is a path segment of l. This equation can also be concisely formulated as a matrix-vector product that describes the travel times for all ray paths

$$\mathbf{t} = \boldsymbol{L}\mathbf{s} \qquad (5)$$

where $\mathbf{t}$ is the travel time vector for the N measured ray paths and $\mathbf{s}$ is the slowness vector containing the slowness values s_j. The $N \times M$ matrix $\boldsymbol{L}$ is the so called path matrix. The elements L_{ij} are the path lengths of the i:th ray through the j:th element. Each ray only covers a few cells, generally making this matrix sparse. The travel time estimation method used here is the path method by Moser (1991). The ray paths are restricted to the edges of the triangular mesh and since only the paths created by the mesh can be used, the travel times will be overestimated. The overestimation can be reduced by increasing the mesh refinement. Dijkstra's algorithm is chosen as it enables the problem to be solved in accordance with Huygens principle and it can be rapidly implemented and solved on a modern computer. Dijkstra's algorithm finds the shortest paths from the mesh node where the source of the P-wave is located to the other nodes at the surface, through the mesh, constructing the $\boldsymbol{L}$-matrix.

Inversion

The inversion scheme is based on several triangular meshes. A coarse and resolution-dependent parameter mesh represents the cells where resistivities and velocities are to be determined. On a refined mesh the forward calculations are carried out using a secondary potential approach. Additionally, for ERT primary fields are obtained through a simulation using a highly refined primary field mesh. The employed inversion method uses the Gauss-Newton method with inexact line search by using the methodology developed and demonstrated by Günther et al. (2006).

Geophysical point data d_i, i.e. apparent resistivities for ERT and travel times for refraction, are stored in a data vector $\mathbf{d} = (d_1, ..., d_D)$ with the length D. Parameter distribution, i.e. resistivity and velocity, is represented by a number of M model parameters m_j yielding the model vector $\mathbf{m} = (m_1, ..., m_M)$. The forward response vector of a model $\mathbf{m}$ is described as $\mathbf{f}(\mathbf{m})$. The task of minimizing the difference between the data and model response is performed with respect to the l_2-Norm, yielding the least-squares method. In order to account for the data errors ϵ_i an appropriate weighting is used resulting in the minimization of the data objective function

$$\phi_d(\mathbf{m}) = \sum_{i=1}^{D} \left| \frac{d_i - f_i(\mathbf{m})}{\epsilon_i} \right|^2 = ||\mathbf{D}(\mathbf{d} - \mathbf{f}(\mathbf{m}))||_2^2 \qquad (6)$$

$$\text{with} \quad \mathbf{D} = \mathrm{diag}(1/\epsilon_i).$$

The process of model updating begins with a starting model $\mathbf{m}^0$, subsequent models $\mathbf{m}^{k+1}$ are then obtained by

$$\mathbf{m}^{k+1} = \mathbf{m}^k + s^k \Delta \mathbf{m}^{\mathbf{k}}.$$

where $\Delta \mathbf{m}^{\mathbf{k}}$ is the model update and s^k a line search factor.

The model has to be constrained in order to produce a unique solution. In order to constrain the model, a functional Φ_m is constructed and weighted by the regularization parameter λ, according to:

$$\Phi = \Phi_d + \lambda \Phi_m \rightarrow \text{ min where } \quad \Phi_m = \|\boldsymbol{C}\mathbf{m}\|_2^2.$$

$\boldsymbol{C}$ is a derivative operator of first order. Application of the Gauss-Newton method leads to

$$\Delta \mathbf{m}^{\mathbf{k}} = \left(\boldsymbol{J}^{\boldsymbol{T}} \boldsymbol{D}^{\boldsymbol{T}} \boldsymbol{D} \boldsymbol{J} + \lambda \boldsymbol{C}^{\boldsymbol{T}} \boldsymbol{C}\right)^{-1}$$
$$\left(\mathbf{J}^{\mathbf{T}} \mathbf{D}^{\mathbf{T}} \mathbf{D} \left(\mathbf{d} - \mathbf{f}(\mathbf{m})\right) - \lambda \boldsymbol{C}^{\boldsymbol{T}} \boldsymbol{C} \mathbf{m}\right) \qquad (7)$$

This equation is solved until Φ plateaus. If data errors are well chosen, the regularization parameter controlling the smoothness of the model should be chosen such that the chi-square value $\chi = \sqrt{\Phi_d / N}$ approaches 1.

When initializing the inversion, a proper parametrization must be made that is fine enough to reflect resolution properties and ensure accurate forward calculations The parametrization is determined by the sensor and shot positions in combination with the approximated depth.

The model values for the resistivity are $\log \rho[\Omega\mathrm{m}]$ and $\log s[\mathrm{s/m}]$ (slowness) for the refraction. The corresponding data values are apparent resistivities $\log \rho^a$ for resistivity and travel times t for refraction.

Structurally coupled inversion

The structurally coupled inversion approach used here requires no canonization of a final main earth model, but the coupled inversion leads to two models, one for each employed method. The overall methodological approach is depicted in Figure 1.

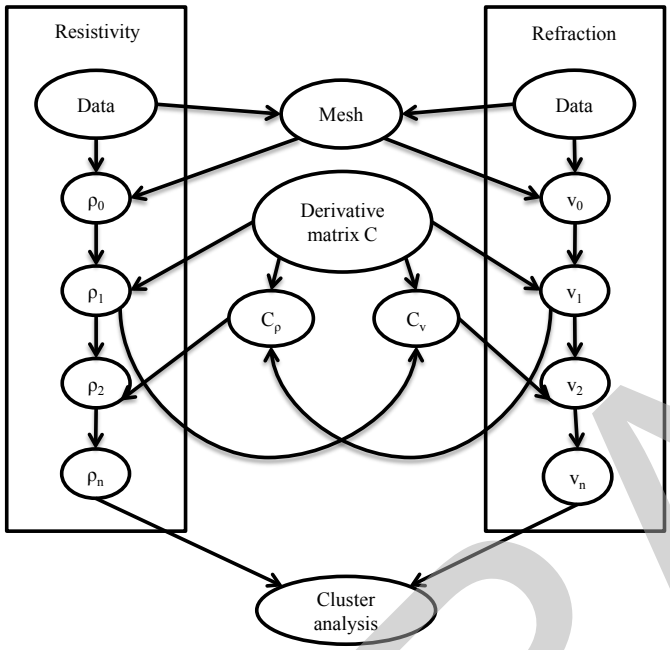

Figure 1: Schematic view of structurally coupled inversion approach leading to cluster analysis.

The roughness operator $\mathbf{C} \in R^{(B)\times M}$ consists of B lines where B is the number of boundaries. Each line is weighted by a diagonal matrix spanned up by a vector $\mathbf{w_c}$

$$\mathbf{C} = \mathrm{diag}(\mathbf{w^c})\mathbf{C_0}\,. \tag{8}$$

The individual elements w_i^c describe the penalty factors for the individual model boundaries, this enables the control of the model characteristics regarding vertical and horizontal structures. It also enables the integration of sharp boundaries or may be exploited to iteratively reinforce structures using an iterative L_1-norm mapping (Claerbout and Muir, 1973).

We now want to apply this principle for exchange of structural information. Let $\mathbf{r^1} = \mathbf{C}(\mathbf{m^1})$ be the roughness vector of one model $\mathbf{m^1}$. We now want to define a function that is 1 (normal penalty) for small gradients and goes to 0 for increasing absolute values of gradients. Günther and Rücker (2006) used an iteratively reweighted least squares (IRLS) function (Claerbout and Muir, 1973). However, we observed that only the main gradients lead to significant reduction of the function and follow Günther et al. (2010) that applied the function

$$w_i = \left(\frac{a}{|r_i| + a} + b\right)^c \tag{9}$$

The value a is a small value representing a negligible gradient. Structural coupling is then achieved by mutually using the weighting functions for constraining the other model. The parameter a controls the point where the roughness r is large enough to influence the constraint weight w. The parameter b may be used to move the curve up and down, an increase of b will move the curve upwards and hence increasing the overall value of the constraint weight w. The parameter c may be used to control the coupling strength, where a large c will result in an overall larger influence of the coupled model. The behavior of this function is clearly illustrated in Figure 2.

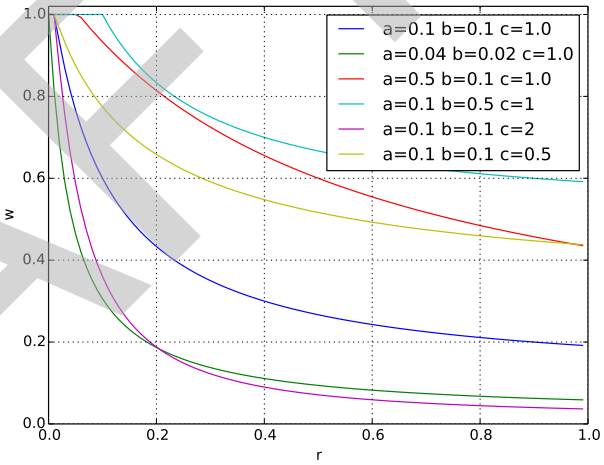

Figure 2: Overview graph to illustrate the behavior of equation 9 for a few combinations of the terms a, b and c.

The constraint weights may be illustrated by plotting them as lines between adjacent model cells as illustrated in Figure 3. Change occurs predominately in the vertical direction for this figure, cells that are more strongly coupled are illustrated by longer lines between these cells, situated between the centers of the these cells.

The procedure starts with the creation of a triangular mesh. The electrodes, geophones and shot points are included as nodes in the mesh. Two separate starting models, resistivity model ρ_0 and velocity model v_0 are created. The constraint matrix $\mathbf{C}$ is created and used in the calculation of the first two models, ρ_1 and v_1. The next step initializes the exchange of structural information between the two model domains. The resistivity model ρ_1 is used to modify the velocity roughness matrix $\mathbf{C}_v$ and the velocity model v_1 is used to modify the resistivity roughness matrix $\mathbf{C}_\rho$. This procedure continues iteratively until we converge at the final models ρ_n and v_n.

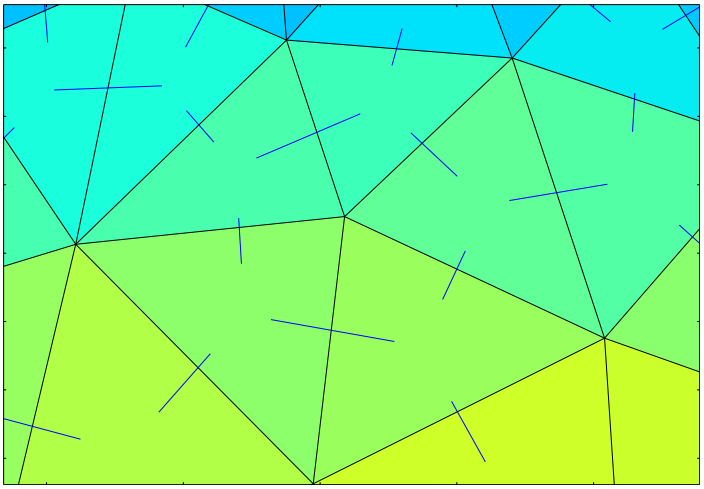

Figure 3: A schematic zoomed view of the constraint weights between model cells

Cluster analysis

The basic idea behind clustering is to group data that share similarities in the model parameters and conversely to differentiate data that share no similarities. Clustering can be seen as a sort of unsupervised learning. There are several ways to learn and there are several cluster algorithms, and the choice of algorithm depends on the application.

As discussed earlier this is the expectation for seismic P-wave velocity and electrical resistivity that are related through e.g. porosity. There are several cluster algorithms that could be applied to seismic and resistivity data. The Fuzzy C-means (FCM) algorithm, that groups a number of data points in an arbitrary-dimensional space into clusters, has successfully been applied to geophysical data by Paasche et al. (2006). We have chosen to apply the k-means algorithm (e.g., Ghosh and Liu, 2009) as it shows promise when inverting for the synthetic models constructed. The k-means has a major setback, which is also common with many other clustering algorithms, in the need to know the number of clusters, or in this case the number of geophysical units that make up our dataset. This requires the use of a-priori information in order to set up the analysis.

An estimate of the number of regions to use can be obtained by analyzing the minimum number of clusters needed to adequately explain the data. This can be done by observing how the χ^2 changes when the number of clusters increase, as is illustrated in Figures 7, 12 and 15. These figures show the χ^2-values for both geophysical methods plotted against the number of clusters.

RESULTS

The results section contains two synthetic models and one field example. The purpose of the two synthetic models is to verify the performance of the methodology towards synthetic data resembling field conditions. The purpose of the field example is to show that the methodology also works with actual field data.

Synthetic model 1

Description

Model 1 is 400 meters long and consists of 3 layers with seismic velocities and resistivities that both increase with depth. The model is inspired by a previous investigation Wisén et al. (2008). It is a fairly typical geological sequence in Scandinavia. The bottom model layer is bedrock with a resistivity of 3000 Ωm and a P-wave velocity of 5000 m/s. The second and intermediate layer is a coarse grained glaciofluvial layer with a resistivity of 250 Ωm and a P-wave velocity of 1700 m/s. The third and uppermost layer is a clay layer with a resistivity of 30 Ωm and a P-wave velocity of 1400 m/s. The top layer has a uniform thickness of 10 m and the intermediate layer has an undulating topography, ranging from 4 to 40 meters in thickness. The bedrock is an infinite half-space below the mid layer. The model is illustrated in Figure 4, and the parameters are presented along with the results in table 1.

The resistivity model is created by simulating an 81 electrode layout with five meter spacing, using a multiple gradient array. Gaussian errors of 3 % were added to the 1019 points of resistivity data according to $\rho_a^{noisy} = \rho_a(0.03n + 1)$ where $n \sim \mathcal{N}(0, 1)$. The refraction seismic model is created by simulating that the geophones were placed at the exact same position as the electrodes, with every fifth geophone used as a shot-point. Gaussian errors with zero mean and standard deviation of 1 ms were added to the 1360 points of refraction data (first breaks).

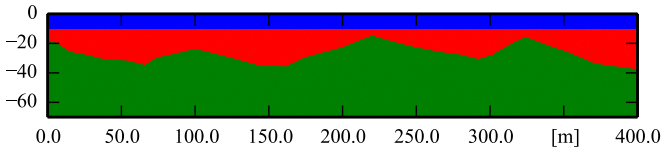

Figure 4: Schematic view of synthetic model 1.

Inversion and statistical comparison

The results from the separate inversions are presented in Figure 5a. The results from the structurally coupled inversions are presented in Figure 5b. The three layers are very well defined in the resistivity section, although the depth penetration fades out quite fast due to the low resistivity in the top. In the lower plot in Figure 5b, the P-wave refraction tomography nicely delineates the bedrock layer but produces a somewhat undulating top layer where boundaries are unclear. The inverted values are in the right range, with some notable overestimations of the P-wave velocity in some regions. The inverted sections are very similar in appearance and the differences are most

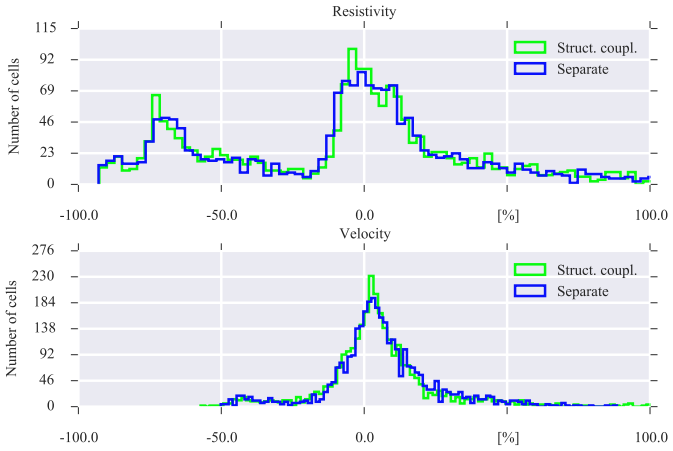

Figure 6: Model 1 histogram plots of relative deviations. The comparison is done for each covered cell. A narrow peak centered close to zero indicates a good resemblance to the synthetic model.

clearly pointed out by the statistical comparison presented in figure 6.

The histograms plotted in Figure 6 visualizes a final model comparison between separate and structurally coupled inversions in relation to the true model. This is accomplished by using the inversion mesh and projecting the known model values onto this mesh. Each true model cell value is then subtracted from the inverted model cell value and divided by the true model cell value, $d_{relative} = \frac{m_{inverted} - m_{true}}{m_{true}}$. This results in a relative deviation in percent for each cell. All compared deviations are then presented in a histogram. With a inverted model in total agreement with the true model, the histogram would show a single spike at 0 % containing all of the compared cells.

The histogram plots in Figure 6 (top) show an improvement in the resistivity results when using the structural coupling. There are more cells with lower relative deviation, i.e. the peak is narrower and higher and is centered closer to zero. This indicates a high degree of similarity between the true synthetic model and the inverted model. The seismic refraction histograms are more or less identical, regardless of whether structural coupling is used or not.

Cluster analysis and cluster plot

The results from the k-means cluster analysis are plotted in Figures 8a and 8b, true and estimated values presented in table 1. They illustrate the results from the separate and structurally coupled inversions respectively. Ideally, the structural coupling should increase the correlation between the parameters, with less scatter in the cross-plot. However, in this case, it is difficult to see such an effect. The number of clusters have been chosen manually, since the number of regions are known in advance. Had the number of clusters not been known beforehand, it could

Table 1: Model 1 layer values.

Value type	Resistivity [Ωm]	P-wave vel. [m/s]
Model value	30	1400
Cluster value (separate)	37	1506
Cluster value (struct. coupl.)	38	1490
Model value	250	1700
Cluster value (separate)	180	2168
Cluster value (struct. coupl.)	176	2161
Model value	3000	5000
Cluster value (separate)	894	4369
Cluster value (struct. coupl.)	1022	4328

be derived from Figure 7, where it is apparent that the minimum number of clusters needed for this dataset is 3.

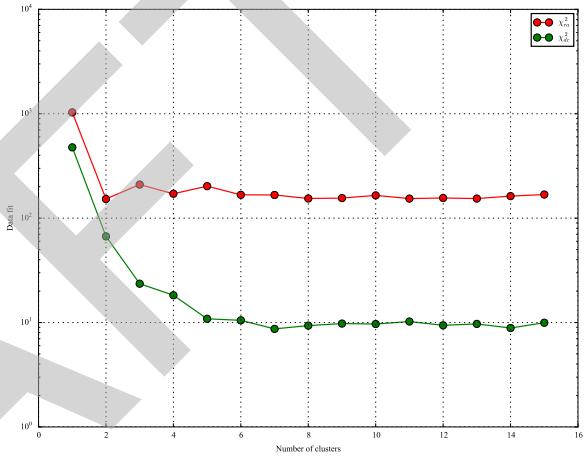

Figure 7: Data fit vs. number of clusters. Illustrating the minimum number of clusters needed to explain the data for model 1.

Synthetic model 2

Description

Model 2 is inspired by the field case presented in this chapter. It is a $500m$ long, two-layer model with a vertical feature, as illustrated in Figure 9. The top layer has a resistivity of $\rho = 30\Omega m$ and a P-wave velocity $V_P = 1000m/s$. The bottom layer has $\rho = 1000\Omega m$ and $V_P = 5000m/s$. The vertical structure has $\rho = 200\Omega m$ and $V_P = 3000m/s$.

Gaussian errors were introduced into the simulated travel-time data and apparent resistivities in the same way as for model 1.

Inversion and statistical comparison

In Figure 10a the results from the separate inversion is shown. The correspondence to the synthetic model in Figure 9 is clearly noticeable in both the resistivity and refraction section. In Figure 10b the two structurally coupled sections are shown. The correspondence to the synthetic

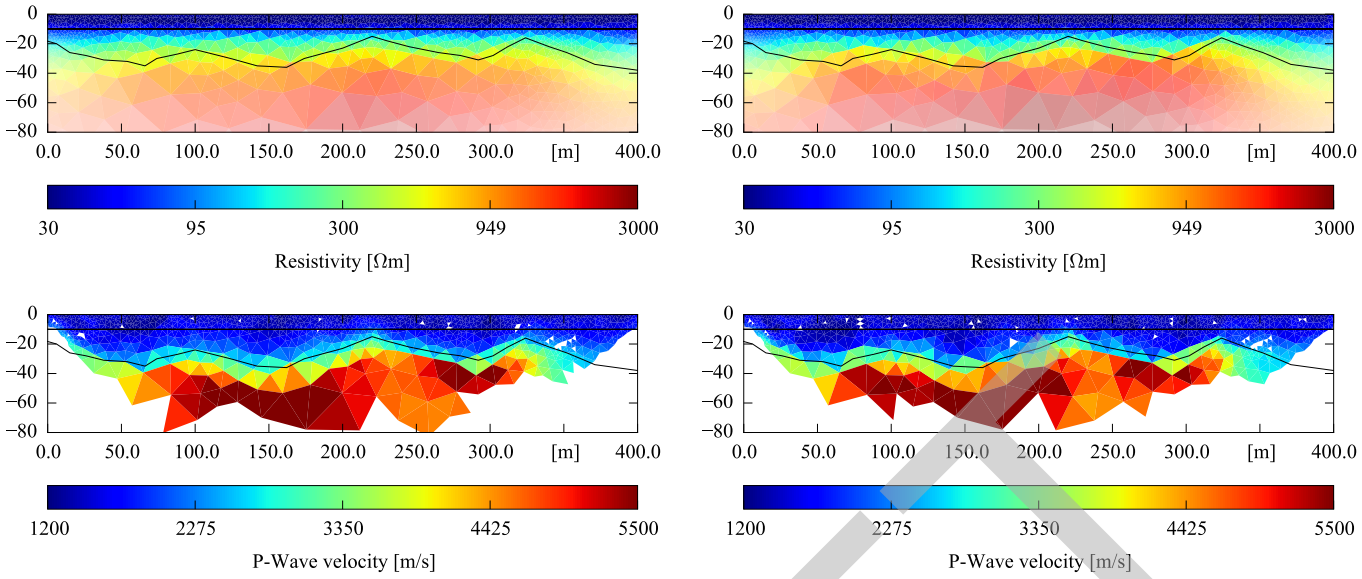

(a) (b)

Figure 5: Model 1 inverted profiles. a) Separate resistivity section, RRMS $\approx 3.01\%$, $\chi^2 \approx 1.01$ and refraction section, RMS $\approx 1.03ms$, $\chi^2 \approx 0.94$. b) Structurally coupled resistivity section, RRMS $\approx 3.08\%$, $\chi^2 \approx 1.06$ and refraction section, RMS $\approx 1.12ms$, $\chi^2 \approx 1.10$.

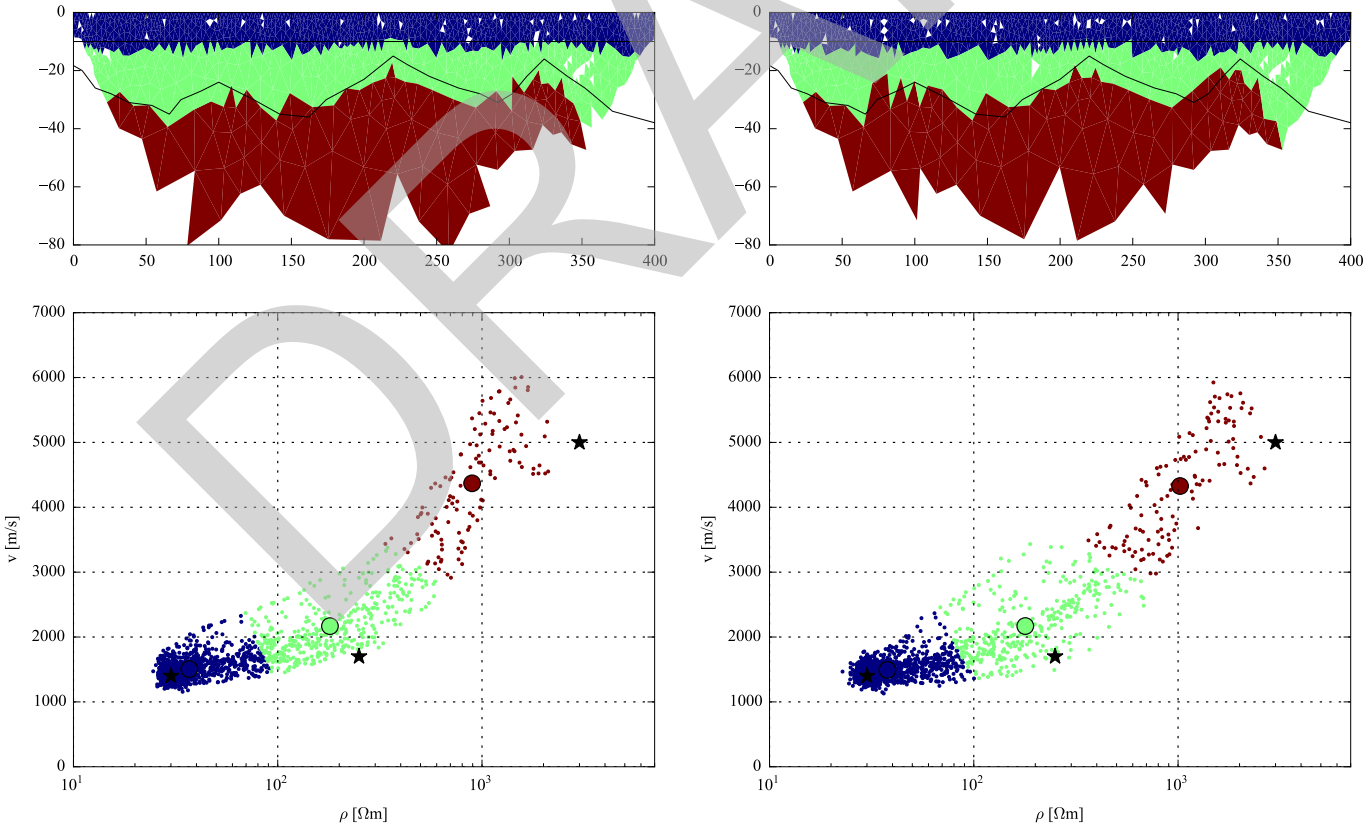

(a) (b)

Figure 8: Model 1 cluster plots of a) separate inversions and b) structurally coupled inversions. Star denotes the synthetic model values, ring denotes the values computed by the k-means cluster analysis. The values can be found in Table 1.

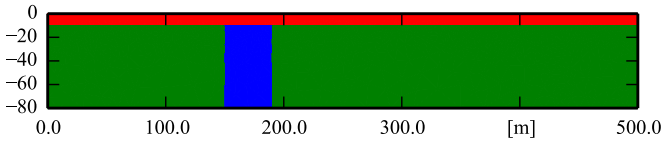

Figure 9: Schematic view of synthetic model 2. The model is inspired by the ESS field case, that is presented later in this article.

model in Figure 9 is in agreement with the results from the separate inversions. There is some smoothing of the boundaries, but in general the different regions are well defined. The values of the cells in the inverted models are in the right range, with a general tendency of overestimation.

Studying the histograms in Figure 11 we can again see an improvement in the resistivity deviations when using the structural coupling. The peak is not narrowed, but it is shifted towards zero, indicating a better correspondence with the original model. The refraction histogram is slightly widened, but it remains centered at zero.

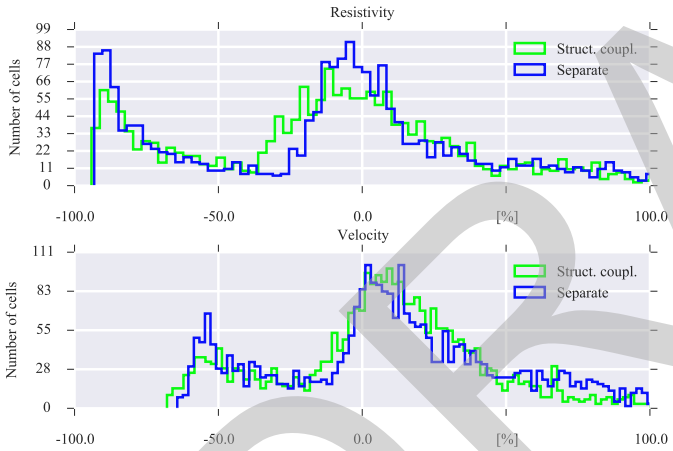

Figure 11: Model 2 histogram plots of relative deviations for each cell. Both resistivity (top) and P-wave velocity (bottom) are shown. A narrow peak centered close to zero indicates a good resemblance to the synthetic model.

Cluster analysis and cluster plot

The cluster plots in Figure 13a and 13b show the improvement that structural coupling can provide. There is greater correlation between the resistivity and the seismic velocity when using the structural coupling as shown by the reduced scatter in the cluster plot. As a result, the estimated cluster centers are also closer to the true positions. The number of clusters have been chosen manually, since the number of regions are known in advance. If the number cluster are not now known beforehand, there is a possibility of testing the minimum number of clusters

Table 2: Model 2 layer values.

Value type	Resistivity [Ωm]	P-wave vel. [m/s]
Model value	30	1000
Cluster value (separate)	34	1294
Cluster value (struct. coupl.)	34	1236
Model value	200	3000
Cluster value (separate)	130	2566
Cluster value (struct. coupl.)	156	2593
Model value	1000	5000
Cluster value (separate)	518	4698
Cluster value (struct. coupl.)	657	4854

needed to fit the data, this is illustrated in figure 12. This figure clearly shows how the χ^2-values develop over the iterations, stabilizing at three clusters.

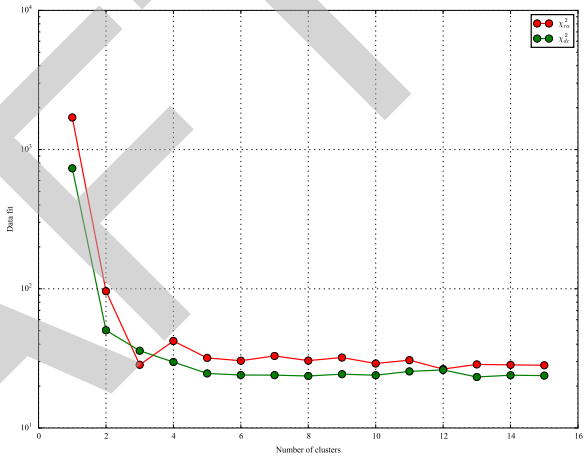

Figure 12: Plot of data fit vs. number of clusters ranging from 1 to 15 clusters. The curves indicate the minimum number of clusters needed to explain the data for model 2.

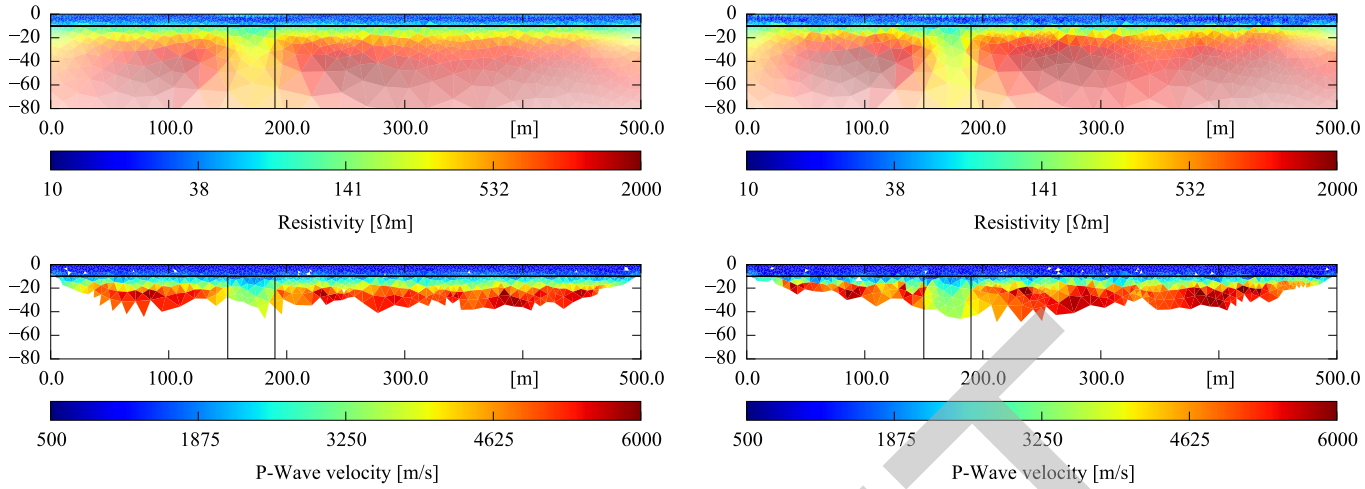

(a) (b)

Figure 10: Inverted sections for model 2. a) Separate resistivity inversion, $\chi^2 \approx 1.09$, RRMS $\approx 3.13\%$ and refraction inversion, $\chi^2 \approx 0.99$, RMS $\approx 1.05ms$. b) Structurally coupled resistivity inversion, $\chi^2 \approx 1.11$, RRMS $\approx 3.13\%$ and refraction inversion, $\chi^2 \approx 1.22$, RMS $\approx 1.2ms$.

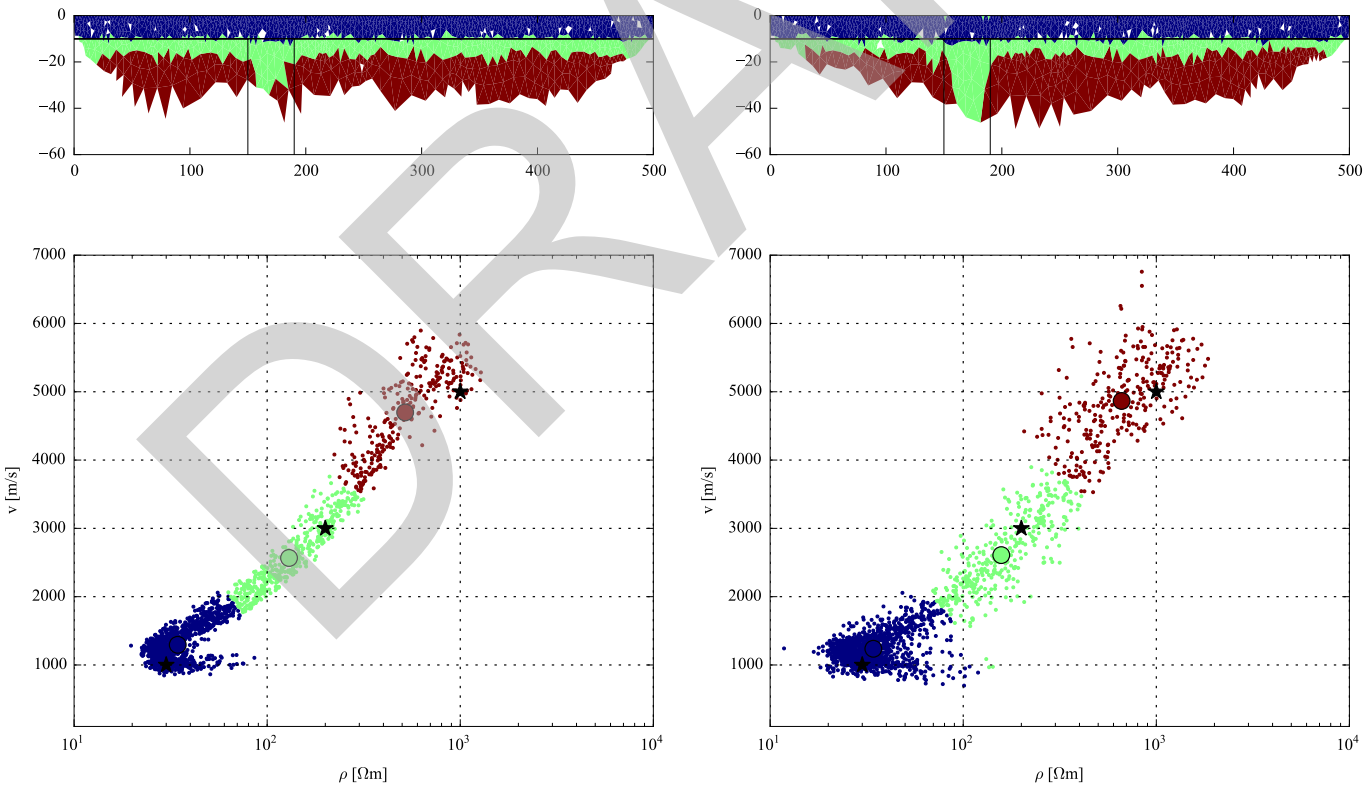

(a) (b)

Figure 13: Model 2 cluster plots of a) separate inversions and b) structurally coupled inversions. Star denotes the synthetic model values, ring denotes the values computed by the k-means cluster analysis. The values can be found in Table 2.

Field case - ESS

Description

The field case is from the site of the European Spallation Source (ESS) in the outskirts of Lund. The site is characterized by a clay till layer of about 10 to 15 meters thickness on top of bedrock. There are dolerite intrusions in the area.

The measurements consist of one 500 m long resistivity profile with 5 m spacing, and one 470 m long refraction seismic profile with 2.5 m spacing. The two profiles are coincident, with an extra geophone between each electrode position. The profiles were positioned so that they would cover at least one dolerite dike.

Inversion

In Figure 14a and in Figure 14b the top layer is nicely resolved in both the resistivity and refraction sections. There is also an indication of a lower resistivity and velocity zone at about 150 m, a dolerite dike. Another indication of a similar structure is found, starting at about 360 m. This is most likely a second dolerite dike.

Cluster analysis and cluster plot

Because there seems to be some spatial correlation of changes in velocity and resistivity we make the assumption that a structural coupling will be useful in this case. Figures 16a and 16b show the cluster plots for the separate and the structurally coupled inversions respectively. Again, the coupling has led to a more pronounced correlation between the parameters, manifested as less scatter.

The number of clusters was set to 4 as indicated by the plot in Figure 15. This also corresponds to a result that is in accordance with the expected geological structure at the site. There is another significant improvement in data fit when using 11 clusters. We chose not to use this many clusters because the drop is only observed for the resistivity. Furthermore, we feel that 11 clusters yield a model that is too complex and thus defeating the purpose of using cluster analysis.

Core drilling and soil-rock penetration testing

Core drilling and soil-rock penetration testing were carried out before the geophysical measurements presented herein were performed. The classifications were obtained from unpublished geotechnical reports associated with the construction of the ESS facility. Both the geophysical and geotechnical results indicate a similar depth to bedrock, as seen in Figures 14 and 16.

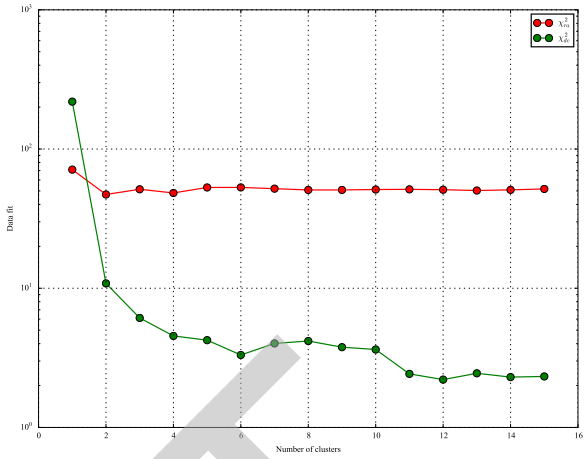

Figure 15: Data fit vs. number of clusters. Used as a tool to indicate the minimum number of clusters needed to explain the data for the ESS field case.

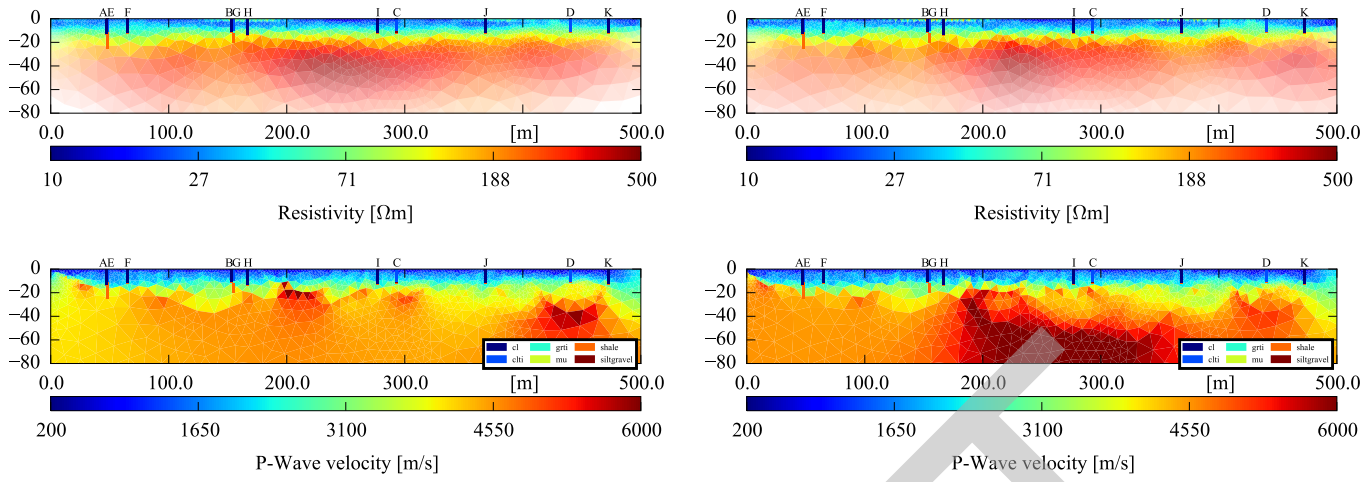

(a) (b)

Figure 14: Field case inversions. a) Separate resistivity inversion section, RMS $\approx 3.41\%$, $\chi^2 \approx 0.92$ and refraction inversion, RMS $\approx 1.33ms$, $\chi^2 \approx 1.65$. b) Structurally coupled resistivity inversion section, RMS $\approx 3.95\%$, $\chi^2 \approx 1.14$ and refraction inversion, RMS $\approx 1.33ms$, $\chi^2 \approx 1.65$. Also included in the plots are geotechnical results. These are plotted as vertical bars, and each bar represents one in-situ test point. A-D are core drillings, E-K are soil-rock soundings.

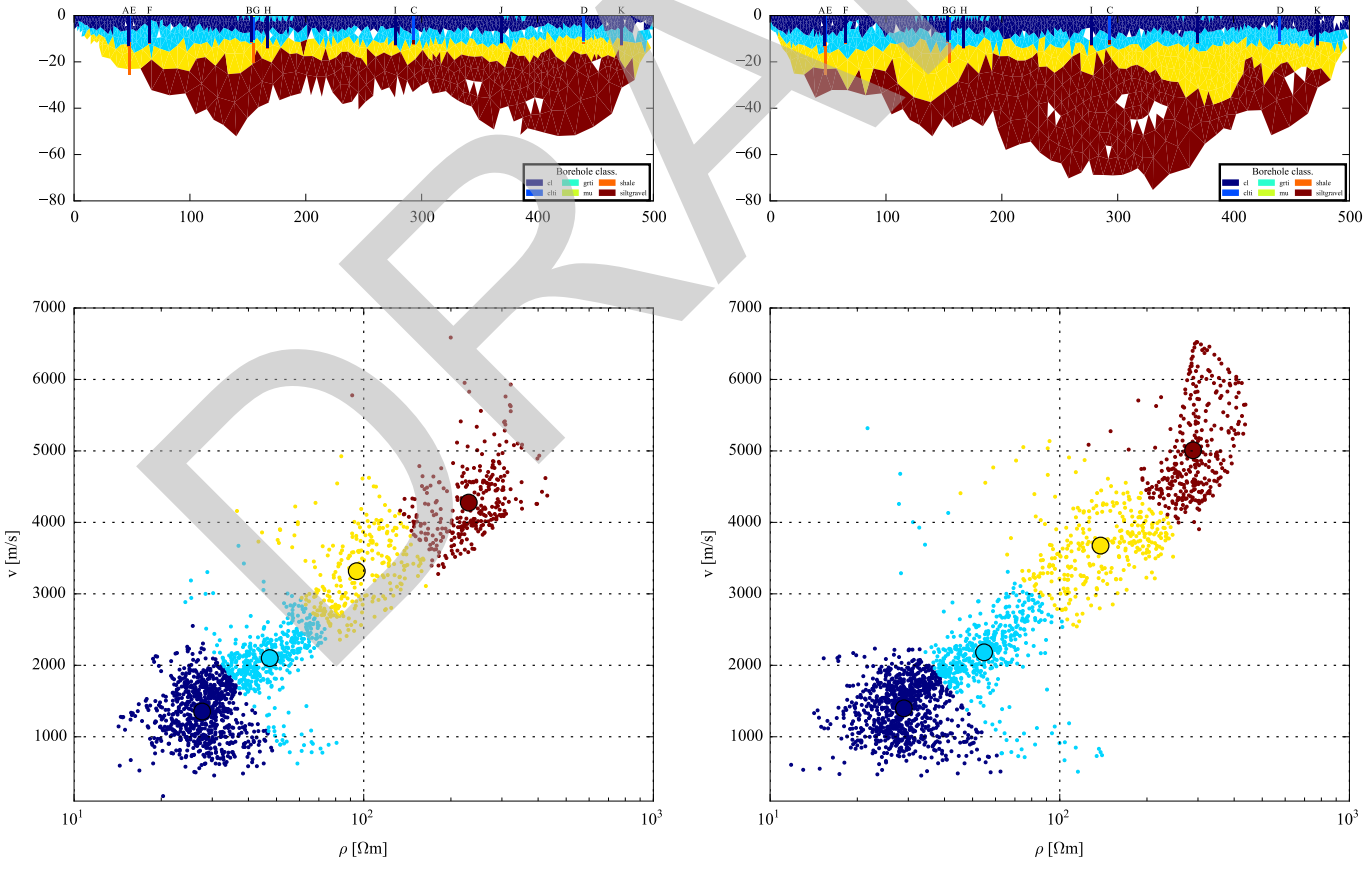

(a) (b)

Figure 16: Cluster plots of the ESS field case. Ring denotes the center values computed by the k-means cluster analysis. Again, the geotechnical results are included. A-D are core drillings, E-K are soil-rock soundings.

CONCLUSIONS

Structurally coupled inversion can enhance the interpretation of the geophysical structure and help to interpret the combined geophysical results. The results obtained from the synthetic models show that our inversion algorithm, which allows for exchange of structural information between e.g. resistivity and seismic refraction, can indeed be beneficial for the ability to delineate layers and structures in the subsurface. The equivalence problem is addressed, and alleviated, by the fact that more than one geophysical method is used. The use of the algorithm relies on the assumption that the contrasts in the parameters, however small, are spatially coinciding. Therefore it is necessary to have an understanding of the local geology, as always.

The results from the field example are promising in the sense that the structurally coupled inversion generates less scatter in the model values. The reduced scatter with the structurally coupled approach may aid both the interpreter and the clustering algorithm.

The use of learning algorithms such as k-means clustering can aid the geophysical interpretation by identifying and enhancing common geophysical contrasts in areas of interest. The examples presented show improvements to the possibilities of automating the characterization of geophysical zones. The main benefits from automation and the use of self-learning algorithms such as the k-means algorithm is not in the improved single geophysical inverted model but instead in the combined cluster section.

A method to automatically determine the number of significant clusters is needed to decrease manual effort and level of subjectivity. We present a very simple but effective way to choose the number of clusters. Further research will be needed into algorithms that can automatically determine the optimal number of clusters in the case of cluster analysis.

Adding more information to aid the inversion should be a way forward, and this could for example be results from down-hole methods such as cross-hole GPR, down hole seismics, CPT-resistivity and geophysical borehole logging. This is an urgent and natural development for the methodology. Such information could provide further insight into the underlying physical explanation such as a change in rock type or degree of weathering.

ACKNOWLEDGEMENTS

This work has been financed by The Swedish Research Council, Formas, (ref no. 2009-797) as part of the GESP project for Environmental Assessment of Road Geology and Ecology in a System Perspective in cooperation with Dept. of Engineering Geology at Royal Institute of Technology (KTH) in Stockholm. Funding was also provided by BeFo, Swedish Rock Engineering Research Foundation, (ref. 314) and SBUF, The Development Fund of the Swedish Construction Industry, (ref. 12718) as part of the Geoinfra-TRUST framework (http://www.trust-geoinfra.se/). Leibniz Institute for Applied Geophysics (LIAG) and Lund University (LU) provided in-kind support. We also wish to thank Niklas Linde and Roger Wisén for providing highly valuable feedback on the manuscript.

REFERENCES

Archie, G. E., 1942, The electrical resistivity log as an aid in determining some reservoir characteristics: I. Petroleum Technology, **5**.

Bedrosian, P., N. Maercklin, U. Weckmann, Y. Bartov, T. Ryberg, and O. Ritter, 2007, Lithology-derived structure classification from the joint interpretation of magnetotelluric and seismic models: Geophysical Journal International, **170**, 737–748.

Bosch, M., 1999, Lithologic tomography: From plural geophysical data to lithology estimation: Journal of Geophysical Research: Solid Earth (19782012), **104**, 749–766.

Cavinato, G., E. Di Luzio, M. Moscatelli, R. Vallone, M. Averardi, A. Valente, and S. Papale, 2006, The new Col di Tenda tunnel between Italy and France: Integrated geological investigations and geophysical prospections for preliminary studies on the Italian side: Engineering geology, **88**, 90–109.

Claerbout, J. F., and F. Muir, 1973, Robust modeling with erratic data: Geophysics, **38**, 826–844.

Dahlin, T., L. Bjelm, and C. Svensson, 1999, Use of electrical imaging in site investigations for a railway tunnel through the Hallandsas Horst, Sweden: Quarterly Journal of Engineering Geology and Hydrogeology, **32**, 163–172. (Part 2 192MA Times Cited:8 Cited References Count:12).

Danielsen, B. E., 2010, The applicability of geoelectrical imaging as a tool for construction in rock: Thesis, Lund University.

Di, Q., and M. Wang, 2010, Determining areas of leakage in the Da Ye Dam using multi-electrode resistivity: Bulletin of Engineering Geology and the Environment, **69**, 105–109.

Dijkstra, E. W., 1959, A note on two problems in connexion with graphs: Numerische mathematik, **1**, 269–271.

Doetsch, J., N. Linde, M. Pessognelli, A. Green, and T. Günther, 2012, Constraining 3-D electrical resistance tomography with GPR reflection data for improved aquifer characterization: Journal of Applied Geophysics, **78**, 68–76.

Gallardo, L. A., and M. A. Meju, 2004, Joint two-dimensional DC resistivity and seismic travel time inversion with cross-gradients constraints: Journal of Geophysical Research, **109**, B03311.

———, 2011, Structure-coupled multiphysics imaging in geophysical sciences: Reviews of Geophysics, **49**.

Ghosh, J., and A. Liu, 2009, 2, *in* K-Means: Chapman and Hall/CRC, Chapman and Hall/CRC Data Mining and Knowledge Discovery Series, 21–35.

Günther, T., R. Dlugosch, R. Holland, and U. Yaramanci, 2010, Aquifer characterization using coupled inversion of MRS & DC/IP data on a hydrogeophysical test-site:

Ext. Abstract, 23. EEGS annual meeting (SAGEEP), April 11-14, 2010; Keystone, CO., 302–307.

Günther, T., and C. Rücker, 2006, A new joint inversion approach applied to the combined tomography of dc resistivity and seismic refraction data: 19. EEGS annual meeting (SAGEEP), Seattle, USA., 433–438.

Günther, T., C. Rücker, and K. Spitzer, 2006, Three-dimensional modelling and inversion of dc resistivity data incorporating topography – II. Inversion: Geophysical Journal International, **166**, 506–517.

Haber, E., and D. Oldenburg, 1997, Joint inversion: a structural approach: Inverse problems, **13**, 63.

Kemna, A., 2000, Tomographic inversion of complex resistivity: PhD thesis, Ruhr-Universität Bochum.

Lelivre, P. G., C. G. Farquharson, and C. A. Hurich, 2012, Joint inversion of seismic traveltimes and gravity data on unstructured grids with application to mineral exploration: Geophysics, **77**, K1–K15.

Linder, S., H. Paasche, J. Tronicke, E. Niederleithinger, and T. Vienken, 2010, Zonal cooperative inversion of crosshole P-wave, S-wave, and georadar traveltime data sets: Journal of Applied Geophysics, **72**, 254–262.

Lines, L. R., A. K. Schultz, and S. Treitel, 1988, Cooperative inversion of geophysical data: Geophysics, **53**, 8–20.

Meju, M., L. Gallardo, and A. Mohamed, 2003, Evidence for correlation of electrical resistivity and seismic velocity in heterogeneous nearsurface materials: Geophysical Research Letters, **30**. (10.1029/2002GL016048).

Moser, T., 1991, Shortest path calculation of seismic rays: Geophysics, **56**, 59–67.

Paasche, H., and J. Tronicke, 2007, Cooperative inversion of 2D geophysical data sets: A zonal approach based on fuzzy c-means cluster analysis: Geophysics, **72**, A35–A39.

Paasche, H., J. Tronicke, K. Holliger, A. G. Green, and H. Maurer, 2006, Integration of diverse physical-property models: Subsurface zonation and petrophysical parameter estimation based on fuzzy c-means cluster analyses: Geophysics, **71**, H33–H44.

Rücker, C., and T. Günther, 2010-2015, Geophysical Modelling and Inversion Library GIMLi - a C++/Python Library for geophysical data analysis.

Rücker, C., T. Günther, and K. Spitzer, 2006, Three-dimensional modelling and inversion of dc resistivity data incorporating topography I. Modelling: Geophysical Journal International, **166**, 495–505.

Tronicke, J., K. Holliger, W. Barrash, and M. D. Knoll, 2004, Multivariate analysis of cross–hole georadar velocity and attenuation tomograms for aquifer zonation: Water Resources Research, **40**.

Vozoff, K., and D. Jupp, 1975, Joint inversion of geophysical data: Geophysical Journal of the Royal Astronomical Society, **42**, 977–991.

Wisén, R., and A. V. Christiansen, 2005, Laterally and mutually constrained inversion of surface wave seismic data and resistivity data: Journal of Environmental & Engineering Geophysics, **10**, 251–262.

Wisén, R., A. V. Christiansen, T. Dahlin, and E. Auken, 2008, Experience from Two Resistivity Inversion Techniques Applied in Three Cases of Geotechnical Site Investigation: Journal of Geotechnical and Geoenvironmental Engineering, **134**, 1730–1742.

Wyllie, M. R. J., A. R. Gregory, and L. W. Gardner, 1956, Elastic wave velocities in heterogeneous and porous media: Geophysics, **21**, 41–70.

Zhang, J., and F. D. Morgan, 1996, Joint seismic and electrical tomography: Proc. EEGS Symposium on Applications of Geophysics to Engineering and Environmental Problems in Keystone, Colorado, 391–396.

ERT and seismic refraction tomography test at Äspö Hard Rock Laboratory

Mathias Ronczka
Lund University, Sweden, mathias.ronczka@tg.lth.se

Roger Wisén, Marcus Wennermark, Torleif Dahlin
Lund University, Sweden

ABSTRACT
Tunnelling below water passages is a challenging task, as fracture zones in the underlying bedrock are often associated with these. Surveys prior to the construction phase that provide information of the subsurface can also be logistically difficult at water passages. An approach that combines refraction seismic and ERT (electrical resistivity tomography) at the Äspö Hard Rock Laboratory (HRL) is presented. The rock laboratory consists of an approximately 2 km long access tunnel and a spiral tunnel that reaches more than 450 m below ground.
The presented surveys cover a water passage along part of the access tunnel which is located around 100 m below the survey line. Seismic and ERT data with co-located sensor positions were collected. The profiles were roughly oriented in north-south direction with a length of about 780 m for ERT and 450 for the seismic survey. A sensor spacing of 5 m was used. Strong power grid noise, the geologic and the test site conditions were logistically challenging for the geophysical surveys. The large resistivity range made it difficult to fit the ERT data appropriately. The unexpected large thickness of the sediments in the southern part of the survey led to a poor signal quality of the seismic data. Nonetheless, inversion results of both data sets are promising, and show that previously unknown geological features can be found by the approach even in an unusually well documented geological environment. The joint interpretation showed that the sedimentary deposits as well as the fracture zones in the northern part could be imaged. A further quality enhancement of the inversion results is possible by including a-priori information and/or a joint inversion of both data sets.

Keywords: Refraction seismic, ERT, joint interpretation.

1 INTODUCTION

The construction of underground structures has attracted much attention recently. They are used for example in the transportation sector to challenge the growth of traffic in and around cities, for underground storage facilities, etc. Detailed subsurface information is essential for a successful completion. A critical point in order to ensure a smooth construction phase is to locate possible weak zones that might slow down the construction progress.

In Sweden, underground infrastructure is mostly built within the crystalline bedrock, where weakness zones are indicated by dry or water bearing fractures. Different methods exist for their location. For example, a set of boreholes give information with a high resolution in depth. Nevertheless, these are very expensive and deliver only punctual information. For the extrapolation into 2D or even 3D geophysical surface based investigations can be used. Recently, Swedish transportation authority's started an increasing number of projects with the aim to develop a scheme of different geophysical methods to map fractures.

Seismic and ERT (electrical resistivity tomography) surveys were conducted to locate fracture zones at the Äspö Hard Rock

laboratory (HRL). In order to increase the reliability of the results, the combination of both methods will be investigated. This can be done for example by a joint interpretation and inversion of both data-sets. Äspö HRL is an underground facility for research and tests around the concept of final disposal of nuclear waste material in hard rock (Rhén et al. 1997), which provides a research opportunity in a well-documented and relatively undisturbed environment also for other branches of research.

2 SITE DESCRIPTION

The Äspö Hard Rock Laboratory is located on the Baltic east coast of Sweden, about 30 km north of Oskarshamn and 400 km south of Stockholm (see Figure 1). The Swedish Nuclear Fuel and Waste Management Company (SKB) started to design a deep final disposal for nuclear fuel. From 1990 – 1995 the excavation of a 3600 m long tunnel that connects the nuclear power plant with the disposal in approximately 450 m depth was conducted. During that phase, a detailed site characterization was done that included geological, hydrogeological and geochemical investigations.

Figure 1: Location of Äspö Hard Rock Laboratory, approx. 30 km north of Oskarshamn

The Äspö bedrock is part of the Trans-Scandinavian Igneous belt (TIB), which extends from southern Sweden towards north and northwest. Mainly granitoids and volcanic rocks can be found in the TIB. Four rock types are dominating: the Äspö diorites, Ävrö granite, greenstone and fine-grained granite. Wikbert et al. 1991 found out that continuous magma-mingling and mixing processes supported the development of dikes and mafic inclusions which form an inhomogeneous rock mass. The crystalline bedrock exhibits porosities of 0.4-0.45 % for the Äspö diorite and 0.23-0.27 % for the fine-grained granite (Stanfors et al. 1999). During the pre-investigation of Äspö HRL, fracture zones were divided into major (width > 5 m) and minor (width < 5 m) ones. The majority of the fractures are oriented northwest-southeast (Berglund et. al 2003), and the most important fractures are depicted in Figure 2. Minerals that fill the fractures were extracted from drill cores and analysed. Thus, unconsolidated material that might have been additionally filling the fractures was probably washed away.

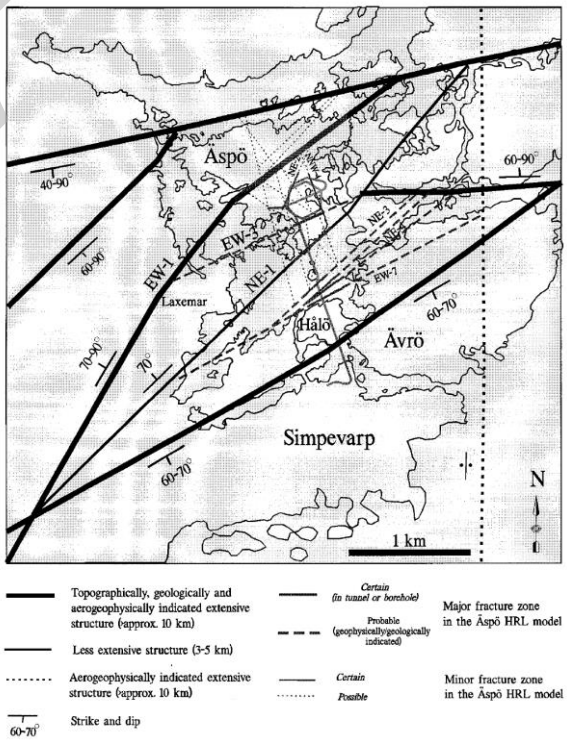

Figure 2: Fracture zones at Äspö HRL (Stanfors et al. 1999).

Calcite, which may be formed by

hydrothermal processes can be used as an indicator for water paths in the rock, (Wikbert et al. 1991). They found out that fractures in N-S and E-W directions could most likely conduct water. The fractures identified as NE-1 crossing the northern part and NE-3 and NE-4, which cross the southern part of the conducted seismic and ERT profile and are of main interest. Quaternary sediments on top of the bedrock are scarce at the Äspö test site. Due to the deep target of the Äspö HRL within the bedrock, no detailed investigation of the Quaternary sediments was done. Vidstrand 2003 stated that the unconsolidated overburden rarely exceeds 5 m thickness and consists mainly of clay, sand and gravel.

4 NUMERICAL MODELLING

The software packages BERT (Boundless Electrical Resistivity) and GIMLi (Geophysical Inversion and Modelling Library) were used for modelling and inversion, (Günther et al., 2006). Inversion was done by a smoothness constrained minimisation. The cost function

$$\Phi = \Phi_d + \lambda\Phi_m = \sum_{i=1}^{N}\left(\frac{d_i - f_i(\mathbf{m})}{\epsilon_i}\right)^2 + \lambda\|\mathbf{C}(\mathbf{m}-\mathbf{m}^0)\|_2^2$$

contains an error-weighted data misfit Φ_d and a model roughness Φ_m weighted with the regularisation parameter λ. The model parameters are hold by $\mathbf{m}$, d_i are the individual data points and $f_i(\mathbf{m})$ the corresponding forward response, weighted by their error ϵ_i. The roughness consists of the derivative matrix $\mathbf{C}$ difference of the model parameter $\mathbf{m}$ towards a reference model $\mathbf{m}^0$, (Günther et al., 2006). Different norms can be used in the cost function like the L_2 norm or the L_1-norm for a robust inversion. Additional model constrains can be incorporated in the object function by extending Φ_m to the weighted model functional

$$\Phi_m = \|\boldsymbol{W_c C m}\|_2^2$$

The weighting matrix $\mathbf{W}_c$ is diagonal and contains the elements w_i^c, which are penalty factors for the different model cell boundaries, (Günther et al. 2006). Very small values correspond to sharp boundaries.

The limited amount of recorded data leads to a non-unique inversion result. Due to the smoothing of the model, which is needed to reduce artificial artefacts for mixed determined problems, it is possible that sharp boundaries cannot be imaged. A structurally coupled joint inversion can reduce these effects by identifying common structures between different methods, (Günther et al. 2006). A schematic sketch of the structurally coupled joint inversion is shown in Figure 3.

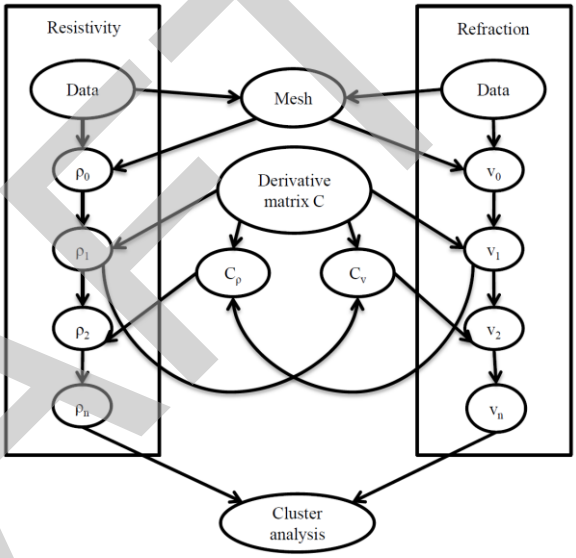

Figure 3: Scheme of the coupled inversion approach, where the roughness C of one inversion is influenced by the other, (Günther et al. 2006)

Forward modelling and inversion are done on unstructured finite element (FE) meshes. For incorporating the sea in the inversion, a region concept was used. The water was assumed to be homogeneous and thus was treated as a single region with a fixed parameter, i.e. resistivity or velocity. Additionally, this region was set to as a background, which lead to better data fits.

(more for the meshes here)

3 FIELD SURVEYS

3.1 Electrical resistivity tomography

ERT measurements were carried out along a

profile in N-S direction directly above the tunnel line. The profile lies between Hålö and Äspö (see Figure 4) to the west of the tunnel line, about 10 m away from a small island. Electrodes were placed onshore and underwater, with a 5 m electrode spacing, along a profile with a length of about 780 m. Data were recorded using the ABEM Terrameter LS instrument. A multiple gradient array was employed to ensure fast progress. The ERT measurement was conducted simultaneously with the seismic survey on 20-24 April 2015.

3.2 Seismic survey

As indicated by Figure 3, seismic refraction data were collected on the sea bed. Hydrophone streamers were laid out with 91 hydrophones using 5 m spacing along a 450 m profile line. For data acquisition the instruments ABEM Terraloc and Geometrics Stratavizor were used, both with 48 channels and with a 5 channel overlap of the two streamers. Hydrophone positions were determined by a differential GNSS, while the topography of the sea bed was mapped with a multibeam echo sounder (Lasheras Maas 2015). For the excitation of seismic p-waves, small explosives were placed approximately 0.5m above the sea bed with a scheduled spacing of 20 m. Due to time constraints not all planed shots were fired and hence there are two small gaps in the data coverage in the northern part of the dataset.

Figure 4: Location of the seismic (red line) and ERT (blue line) profile at Äspö HRL (after Lasheras Maas 2015).

5 RESULTS

About 6700 data points were gathered in the ERT survey. The surveying conditions were challenging with electrodes lying in brackish water as well as on outcropping rock, leading to contact resistances ranging from around 100 Ω to over 100 kΩ. Nevertheless, data quality is generally good judging from apparent resistivity pseudosection plots, although recorded full waveform data reveals high power grid noise levels.

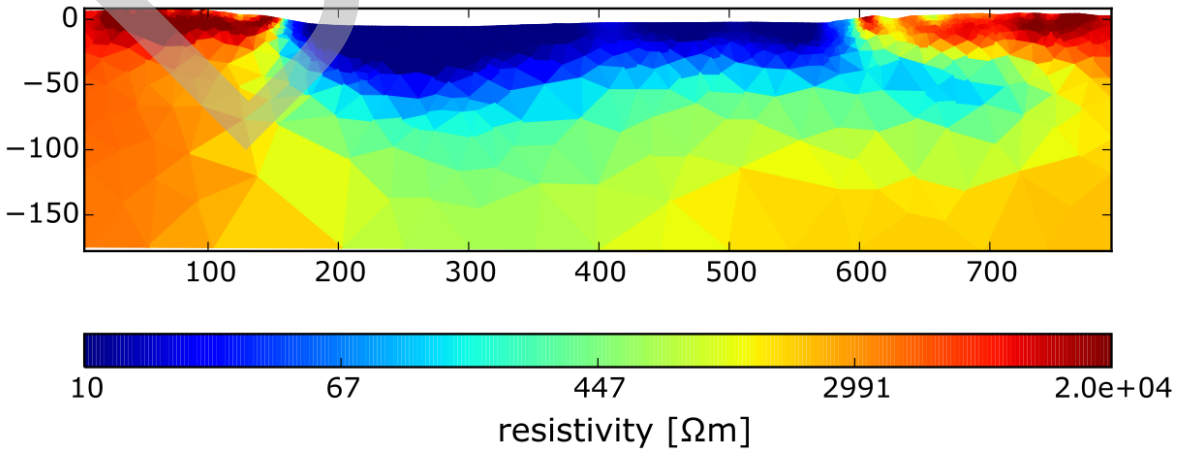

Figure 5: Inversion result of the ERT data set at Äspö HRL.

While processing the raw data, electrodes with an apparently wrong GNNS position were identified and all combinations containing these electrodes deleted. For the inversion an error model consisting of 3% noise and a voltage error of 0.1 mV was used.
Data were interpreted as models of the resistivity distribution via inverse numerical modelling (inversion) using BERT (*add reference*). A smoothness constrained inversion was done with the abort criterion $\chi^2 = \Phi_d/N = 1$, whereas Φ_d is the data misfit and N the data amount. The L1 norm (robust inversion) was used for Φ_d. Although some apparent resistivities that exhibit a high error and/or does not fit into the raw data distribution were deleted. One explanation for the difficult data fit is that the measured apparent resistivity distribution covers several orders of magnitude and that extraordinary high resistivity jumps occur, which is always a challenging task for ERT. It is also expected that 3D effects will occur due to the site characteristics, namely towards the end of the line and in the middle. The corresponding inversion result is given in Figure 4. The sea water was incorporated as a single region with a fixed resistivity of 1.4 Ωm, which is the mean fluid resistivity measurements in three different depths.

Outcrops of the bedrock lead to high resistivities of about 28000 Ωm at the northern and southern end of the profile. A low resistive zone appears at x = 200-600 m, directly below the sea, down to approximately 60-80 m depth, which could possibly be caused by a change of the geologic conditions that could be interpreted as a steep valley filled with sediments. This has not been documented previously. It might be caused by a graben structure formed between the well documented fracture zones NE3 and NE4. At the end of the sea (x = 600 m), a second low resistive zone appears that reaches down to 140 m depth, which correspond with the well-known fracture zone NE1. But is most likely possible that this is caused by 3D effects.
A clear identification for the reason that might cause the low resistive zones can be possibly made using the results of the seismic refraction survey. As stated before, it covers the middle part of the ERT profile below the sea. Prior to the data fitting, negative travel times were deleted. For data inverse modelling, the software GIMLi for geophysical modelling and inversion was used. The fitted p-wave velocity distribution is shown in Figure 5. The crystalline bedrock appears as a high velocity zone of about 5600 m/s. Towards the northern part, the velocity of the bedrock decreases down to 5000 m/s. At the southern part, between x = 200-300 m, the result shows a low velocity zone down to 60 m depth, which is extended towards the north for shallow parts of the model, above 20 m depth. This finding coincides with the low resistive part in ERT result and is interpreted as sedimentary deposits that exhibit low velocities and, if water saturated, low

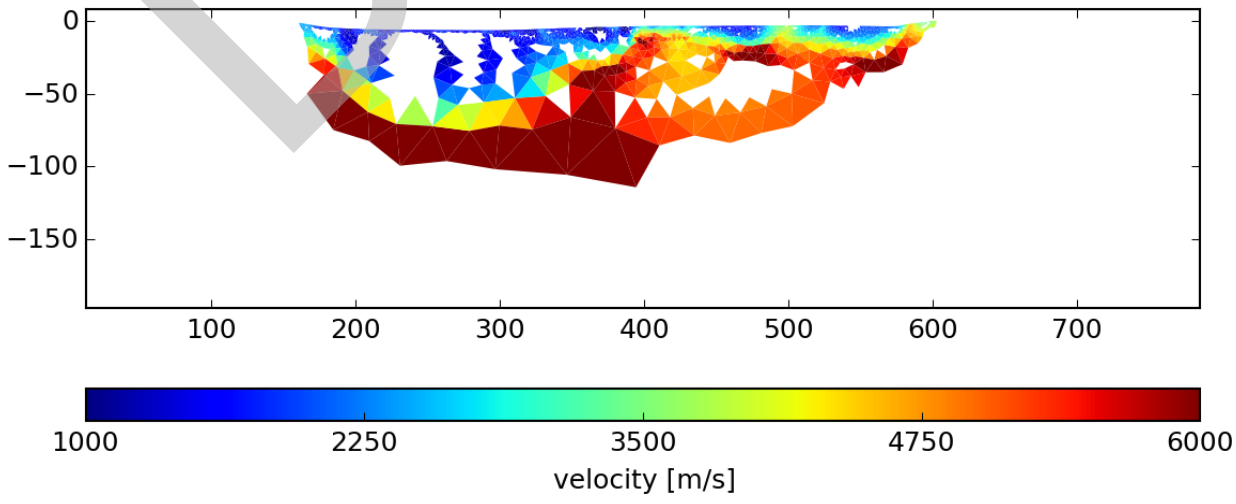

Figure 6: Inversion result of the seismic survey

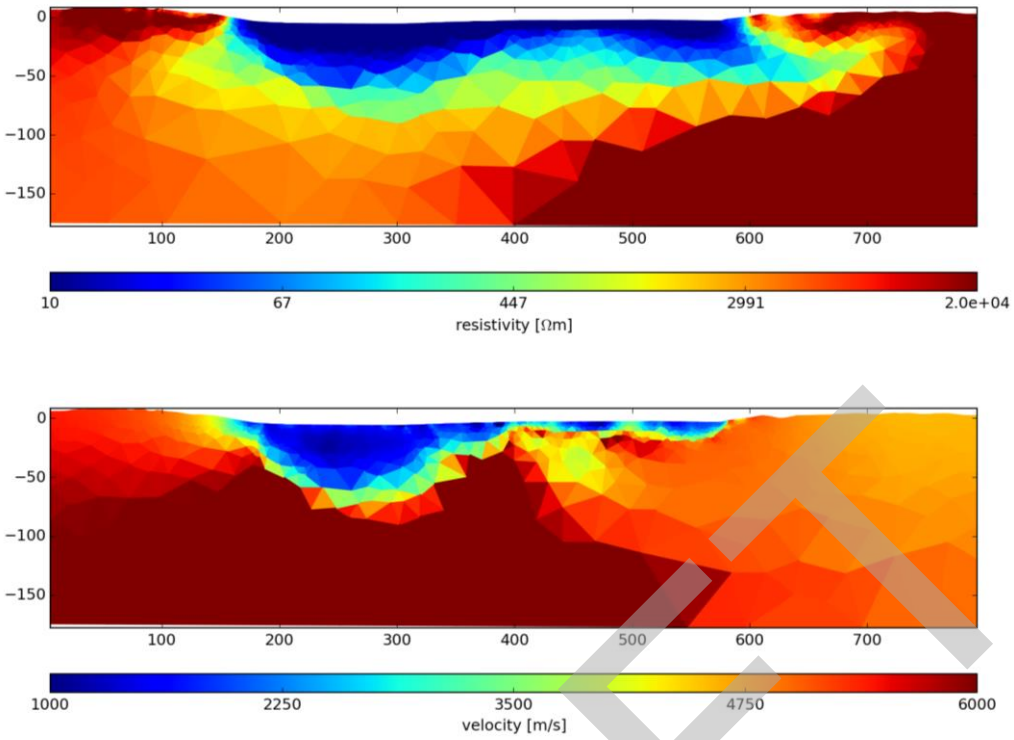

Figure 7. Result of the joint inversion with the resistivity distribution (top) and p-wave velocities (bottom) for the Äspö test site

resistivities. The sediments damp the seismic signal significantly that leads to a poor data quality below the sediments in the southern part. No further low velocity zones at larger depth appear, but at the near surface zone down to approximately 20 m depth. The fracture zone is not visible in the seismic result, due to the low data coverage in this part of the model.

Generally, the interface towards the bedrock below the sedimentary deposits is not exactly resolvable. The bedrock appears with a lower resistivity in this part. In order to improve the inversion results, a joint inversion of the ERT and seismic data set was performed. The coupling was applied starting with the third iteration step. The first two were done separately, in order to use models for the joint inversion that differ from a homogeneous half space. The regularisation parameters were the same as for the separated inversions. The result is shown in Figure 7. The upper picture of Figure 7 shows the ERT result and the bottom picture the seismic result. Due to the coupling, both models could be improved. Compared to the separated inversions, the low resistive zone, which correspond to the sedimentary deposits, now appears thinner than before. Higher resistivities appear below the sediments. The interface between the bedrock and the sediments appears sharper in the seismic result as well. While interpreting the data, it has to be taken into account that 3D effects might influence the result, which cannot be taken into account in a 2D inversion. Lower resistivities still appear between 200m<x<300m, while the seismic result shows the highest velocities. This is very difficult to interpret, due to a low coverage for this model part.

5 CONCLUSION AND OUTLOOK

The inversion of the ERT data shows that the fracture zone in the northern part could be imaged as a low resistive zone. Additionally, a second low resistive anomaly in the southern part appears, which is interpreted as a previously unknown steep sediment valley. A comparison with the seismic result shows a low velocity zone in the same region, which is verification for sedimentary deposits. Due to insufficient data coverage, the fracture zone in the northern part of the profile could not be imaged by the seismic survey. An extension of the profile would be one way to ensure sufficient coverage.

In conclusion the preliminary evaluation shows that the approach has given very promising results, which illustrates that continuous information provided by geophysics can reveal previously unknown geological features even in an unusually well documented geological environment. There are possibilities for further developments of the interpretation of the data without costly additional data acquisition. For example, the reliability of the inversion results can be enhanced by implementing a-priori information, which could confine the ambiguity of the model space. Another possibility is to implement structurally coupled inversion, in which the data from the different geophysical models supports each other to reduce ambiguities.

6 REFERENCES

Berglund, J. et al., 2003. Äspö Hard Rock Laboratory. Update of the geological model. SKB (Swedish Nuclear Fuel and Wast Management Company) P-03-07.

Günther, T., Bentley, L.R. and Hirsch, M. 2006. A new joint inversion algorithm applied to the interpretation of DC resistivity and refraction data. In Proceedings of XVI International Conference on Computational Methods in Water Resources.

Lasheras Maas, N., 2015. Site characterisation at the Äspö Hard Rock Laboratory through seismic refraction, Bachelor Thesis, Lund University, Sweden

Rhén, I. et al., 1997. Äspö HRL-Geoscientific evaluation 1997/2 Results from pre-investigations and detailed site characterization. SKB (Swedish Nuclear Fuel and Waste Management Company) TR-97-03

Stanfors, R., Rhén, I., Tullborg, E.L. and Wikberg, P., 1999. Overview of geological and hydrogeological conditions of the Äspö hard rock laboratory site. Applied Geochemistry, 14(7), 819-834

Vidstrand, P., 2003. Äspö Hard Rock Laboratory. Update of the hydrogeological model 2002. SKB (Swedish Nuclear Fuel and Waste Management Company) IPR-03-35

Wikberg, P. et al., 1991. Äspö Hard Rock Laboratory. Evaluation and conceptual modelling based on the pre-investigations 1986-1990. SKB (Swedish Nuclear Fuel and Wast Management Company) Technical Report 91-22, (June)